

## Key Points:

- New observations of asteroid (16) Psyche's physical properties indicate a different composition and properties than earlier data had shown
- The best current analysis indicates that Psyche's density is 3,400–4,100 kg m<sup>-3</sup>, indicating a mixture of rock with 30–60 vol% metal
- Contradictions in data of Psyche physical properties may not be resolved until the NASA Psyche mission arrives at the asteroid

## Correspondence to:

L. T. Elkins-Tanton,  
ltelkins@asu.edu

## Citation:

Elkins-Tanton, L. T., Asphaug, E., Bell, J. F., III, Bercovici, H., Bills, B., Binzel, R., et al. (2020). Observations, meteorites, and models: A preflight assessment of the composition and formation of (16) Psyche. *Journal of Geophysical Research: Planets*, 125, e2019JE006296. <https://doi.org/10.1029/2019JE006296>

Received 3 DEC 2019

Accepted 29 JAN 2020











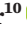



Accepted article online 21 FEB 2020

This article was corrected on 20 APR 2020.

© 2020. The Authors.

This is an open access article under the terms of the Creative Commons Attribution-NonCommercial License, which permits use, distribution and reproduction in any medium, provided the original work is properly cited and is not used for commercial purposes.

## Observations, Meteorites, and Models: A Preflight Assessment of the Composition and Formation of (16) Psyche

L. T. Elkins-Tanton<sup>1</sup> , E. Asphaug<sup>2</sup>, J. F. Bell III<sup>1</sup>, H. Bercovici<sup>1</sup>, B. Bills<sup>3</sup> , R. Binzel<sup>4</sup>, W. F. Bottke<sup>5</sup> , S. Dobb<sup>1</sup>, D. J. Lawrence<sup>6</sup> , S. Marchi<sup>5</sup> , T. J. McCoy<sup>7</sup>, R. Oran<sup>4</sup> , R. S. Park<sup>3</sup> , P. N. Peplowski<sup>6</sup> , C. A. Polansky<sup>3</sup>, T. H. Prettyman<sup>8</sup> , C. T. Russell<sup>9</sup> , L. Schaefer<sup>10</sup> , B. P. Weiss<sup>4</sup>, M. A. Wicczorek<sup>11</sup> , D. A. Williams<sup>1</sup> , and M. T. Zuber<sup>4</sup> 

<sup>1</sup>Arizona State University, Phoenix, AZ, USA, <sup>2</sup>University of Arizona, Tucson, AZ, USA, <sup>3</sup>Jet Propulsion Laboratory, Pasadena, CA, USA, <sup>4</sup>Massachusetts Institute of Technology, Cambridge, MA, USA, <sup>5</sup>Southwest Research Institute, Boulder, CO, USA, <sup>6</sup>Applied Physics Laboratory, Laurel, MD, USA, <sup>7</sup>Smithsonian Institution, Washington, DC, USA, <sup>8</sup>Planetary Science Institute, Tucson, AZ, USA, <sup>9</sup>University of California, Los Angeles, CA, USA, <sup>10</sup>Stanford University, Stanford, CA, USA, <sup>11</sup>Observatoire de la Côte d'Azur, CNRS, Laboratoire Lagrange, Université Côte d'Azur, Nice, France

**Abstract** Some years ago, the consensus was that asteroid (16) Psyche was almost entirely metal. New data on density, radar properties, and spectral signatures indicate that the asteroid is something perhaps even more enigmatic: a mixed metal and silicate world. Here we combine observations of Psyche with data from meteorites and models for planetesimal formation to produce the best current hypotheses for Psyche's properties and provenance. Psyche's bulk density appears to be between 3,400 and 4,100 kg m<sup>-3</sup>. Psyche is thus predicted to have between ~30 and ~60 vol% metal, with the remainder likely low-iron silicate rock and not more than ~20% porosity. Though their density is similar, mesosiderites are an unlikely analog to bulk Psyche because mesosiderites have far more iron-rich silicates than Psyche appears to have. CB chondrites match both Psyche's density and spectral properties, as can some pallasites, although typical pallasitic olivine contains too much iron to be consistent with the reflectance spectra. Final answers, as well as resolution of contradictions in the data set of Psyche physical properties, for example, the thermal inertia measurements, may not be resolved until the NASA Psyche mission arrives in orbit at the asteroid. Despite the range of compositions and formation processes for Psyche allowed by the current data, the science payload of the Psyche mission (magnetometers, multispectral imagers, neutron spectrometer, and a gamma-ray spectrometer) will produce data sets that distinguish among the models.

**Plain Language Summary** Since the NASA mission to asteroid (16) Psyche was selected, interest from the public and from the scientific community in the asteroid has risen considerably. New observations of the asteroid's physical properties indicate a different composition than earlier data had shown. A decade ago, much of the community thought the asteroid was 90% metal on its surface. There are still contradictions in the compilation of all current data, but the best analysis indicates that Psyche's density is between 3,400 and 4,100 kg m<sup>-3</sup>, indicating it is a mixture of rock with between 30 and 60 vol% metal.

### 1. Introduction

Planning for the Psyche mission requires anticipating what features, compositions, and textures the asteroid might have and then further preparing for how those characteristics might be reflected in the eventual mission data. Earth-based observations of (16) Psyche and other asteroids (henceforth, in this paper, we will omit the designator (16)), along with the library of meteorites available on Earth, form the basis for this exercise.

Recent ground observations of asteroid Psyche provide sufficiently mature and consistent shape and size estimates to support trajectory, orbit, and observation planning (Drummond et al., 2018; Shepard et al., 2017; Viikinkoski et al., 2018). However, key characteristics needed to constrain Psyche's origins and evolution, particularly surface and bulk composition, remain poorly known.

While information about the asteroid will continue to accumulate during the mission planning stage, the mission itself is flexible enough to adjust for changing expectations based on the most recent observing

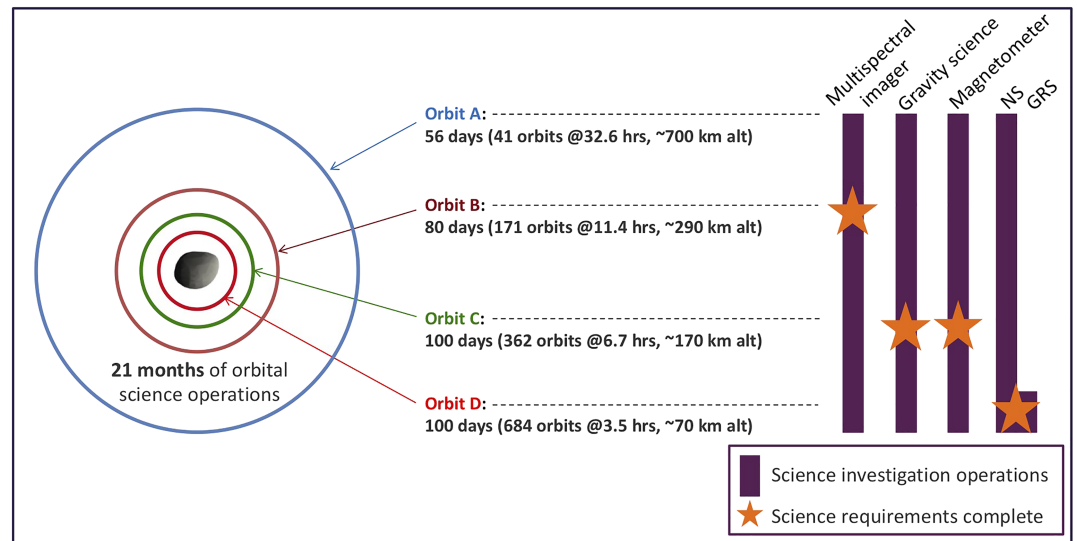


**Figure 1.** The Psyche science orbits provide each science instrument with increasingly higher resolution data as the mission progresses. The gamma-ray spectrometer requires proximity to the asteroid uniquely close among the instruments. When science operations end, the mission is required to have mapped >80% of Psyche's surface to a pixel scale of  $\leq 20$  m; we expect to exceed requirements and even reach a pixel scale under 5 m for some areas of the surface.

data. The Psyche mission leverages the recent experience of the Dawn mission to develop strategies for thoroughly mapping and investigating a new solar system object while adjusting to Psyche's actual physical parameters as they are refined during the orbital operations phase. A series of four circular orbits at progressively lower altitudes are used (Orbits A through D) to investigate Psyche with increasing resolution by the full instrument suite (Figure 1).

The Psyche payload consists of

- Dual fluxgate magnetometers mounted on a 2-m boom in a gradiometer configuration, designed to search for evidence of remanent magnetization;
- Redundant multispectral imagers with eight filters to map composition and geomorphology; and
- A gamma-ray and neutron spectrometer to determine elemental composition.

The mission was designed to allow all instruments to participate together in each science orbit, and the instrument data will be enhanced with a gravity investigation using the spacecraft itself and its X-band radio communications system. For more information about the instruments on the Psyche mission, please see Hart et al. (2018) and Polanskey et al. (2018a).

Applying lessons learned from the Dawn mission (Polanskey et al., 2018b), the Psyche mission profile incorporates increased margins in operations duration, data volume, and onboard data storage capacity, providing a more robust operations environment and greater adaptability to unanticipated aspects of Psyche's physical characteristics. Prelaunch simulations of the credible extremes of all physical parameters are conducted to confirm the viability of the operations plan. Each new set of ground or space-based measurements obtained provides the mission team with additional opportunities to exercise how we will eventually adapt our plans to the Psyche we encounter upon arrival.

In this paper, we will review the current data for asteroid Psyche and discuss possible interpretations. We will place the data and interpretations in the context of possible formation scenarios for Psyche, and then, we will discuss the expectation of mission data to test the resulting possible hypotheses.

## 2. Constraints From Existing Data

### 2.1. Masses, Volumes, and Densities

A key parameter for predicting the composition of an asteroid is its bulk density. Several shape models of Psyche have been derived from high-resolution image, radar, and stellar occultation data. They suggest

**Table 1**  
*Selected Diameters and Volumes of Psyche*

| Effective diameter (km) | Effective volume ( $\times 10^6 \text{ km}^3$ ) | Source                    |
|-------------------------|---|---------------------------|
| 226 $\pm$ 23            | 6.04 $\pm$ 1.84                                 | Shepard et al. (2017)     |
| 223 $\pm$ 7             | 5.81 $\pm$ 0.55                                 | Drummond et al. (2018)    |
| 226 $\pm$ 5             | 6.04 $\pm$ 0.40                                 | Viikinkoski et al. (2018) |

that Psyche has a broadly triaxial shape. The shape model for Psyche is known sufficiently well to have an effective volume agreeing to within about 10% for the three most recent estimates of their central values and within about 30% difference at the extremis of their one sigma errors (Table 1). The studies cited in this table further show that Psyche has approximate principal axes a, b, and c of 290, 245, and 170 km (e.g., Viikinkoski et al., 2018).

The mass of Psyche has been estimated primarily using two different methods. The first method uses astrometrical observations of two or more asteroids acquired before and after close encounters (Baer & Chesley, 2017). These observations are then used to determine their mutual deflections caused by the combined gravitational force of the two bodies. The change in the trajectory of each body is related to their masses. The second method estimates several asteroid masses as part of a global planetary ephemeris solution, which uses all available ground- and space-based astrometry as well as ground-based radio tracking of spacecraft at planets (Konopliv et al., 2011b; Kuchynka & Folkner, 2013). In this case, most of the sensitivity for estimating asteroid masses comes from Mars ranging data.

The density of Psyche has been estimated by a number of researchers (see Table 2 and Figure 2) using mass and shape models. Mass estimates of Psyche have additional uncertainties (see Table 2). Thus, uncertainties in bulk density are compounded from uncertainties in mass. In addition, interpretation of density is hindered by an unknown porosity of Psyche, a porosity that may include all scales from grains to rubble-pile fractures and chasms. The smallest density estimate over the last decade is  $\sim 2,500 \text{ kg m}^{-3}$  and the largest  $\sim 7,600 \text{ kg m}^{-3}$ .

**Table 2**  
*Measured Masses and Calculated Densities for Psyche*

| Mass ( $\times 10^{19} \text{ kg}$ ) | Density <sup>a</sup> ( $\text{kg m}^{-3}$ ) | Density (recalculated) <sup>b</sup> ( $\text{kg m}^{-3}$ ) | Reference   |
|--------------------------------------|---|--|---|
| 1.73 $\pm$ 0.52                      | 1,800 $\pm$ 600                             | 2,860 $\pm$ 880  | Viateau (2000)  |
| 6.72 $\pm$ 0.56                      | 6,980 $\pm$ 580                             | 11,100 $\pm$ 1,200   | Kuzmanoski and Koračević (2002)   |
| 2.67 $\pm$ 0.44                      | na  | 4,420 $\pm$ 780  | Kochetova (2004)  |
| 2.57 $\pm$ 0.34                      | 4,020 $\pm$ 1,360                           | 4,250 $\pm$ 630  | Baer and Chesley (2008)   |
| 3.17 $\pm$ 0.06                      | 3,700 $\pm$ 100                             | 5,240 $\pm$ 360  | Fienga et al. (2009)  |
| 4.59 $\pm$ 1.93                      | na  | 7,590 $\pm$ 3,230  | Somenzi et al. (2010)   |
| 2.27 $\pm$ 0.08                      | 6,730 $\pm$ 3,050                           | 3,760 $\pm$ 280  | Baer et al. (2011)  |
| 2.47 $\pm$ 0.69                      | 7,320                                       | 4,090 $\pm$ 1,170  | Konopliv et al. (2011)  |
| 2.72 $\pm$ 0.75                      | 3,380 $\pm$ 1,160                           | 4,500 $\pm$ 1,280  | Carry (2012)  |
| 2.35 $\pm$ 0.55                      | na  | 3,890 $\pm$ 950  | Kuchynka and Folkner (2013)   |
| 2.23 $\pm$ 0.36                      | na  | 3,690 $\pm$ 640  | Fienga et al. (2014)  |
| 2.29 $\pm$ 0.07                      | na  | 3,780 $\pm$ 280  | Baer and Chesley (2017)   |
| na                                   | 4,500 $\pm$ 1,400                           |  | Shepard et al. (2017) using mass of Carry (2012)                                      |
| na                                   | 3,700 $\pm$ 600                             |  | Hanuš et al. (2017) using mass of Fienga et al. (2014)                                |
| na                                   | 4,600 $\pm$ 1,300                           |  | Hanuš et al. (2017) using mass of Carry (2012)  |
| 2.43 $\pm$ 0.35                      | 4,160 $\pm$ 640                             | 4,020 $\pm$ 640  | Drummond et al. (2018)  |
| 2.41 $\pm$ 0.32                      | 3,990 $\pm$ 260                             | 3,990 $\pm$ 590  | Viikinkoski et al. (2018)   |
| 1.56 $\pm$ 0.14                      | 2,680 $\pm$ 1,210                           | 2,580 $\pm$ 1,150  | Siltala and Granvik (2019) high estimate  |
| 1.48 $\pm$ 0.55                      | 2,540 $\pm$ 980                             | 2,450 $\pm$ 910  | Siltala and Granvik (2019) low estimate   |
| 2.29 $\pm$ 0.14                      |   | 3,780 $\pm$ 340  | This paper: mass based on a modified uncertainty in mass from Baer and Chesley (2017) |

Notes. na indicates the paper did not report their own estimate.

<sup>a</sup>Densities from the reference. <sup>b</sup>Densities recalculated using mass from the reference and volume from Viikinkoski et al. (2018).

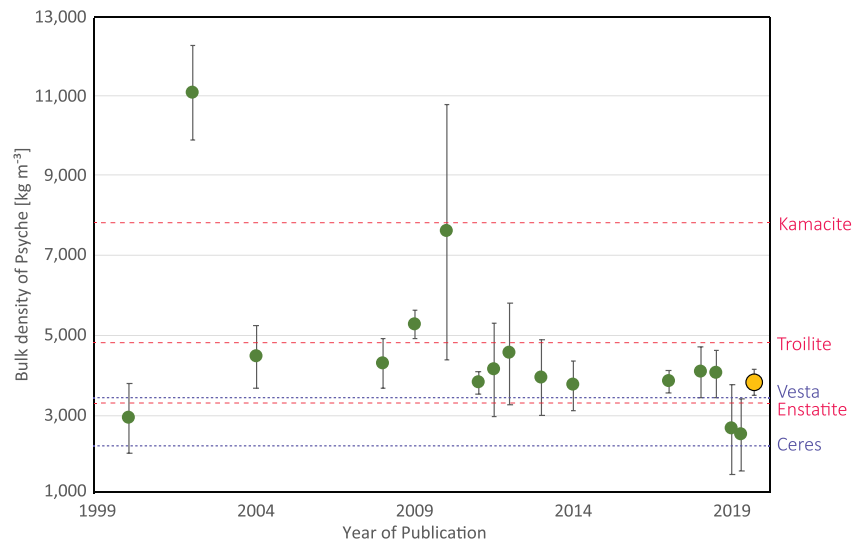


**Figure 2.** Bulk densities of Psyche from Table 2, showing error bars and the focusing of density measurements over time. The preferred value from this paper,  $3,780 \pm 340 \text{ kg m}^{-3}$ , is shown in yellow. For comparison, Vesta's density is  $3,454 \text{ kg m}^{-3}$  (C. T. Russell et al., 2012), and Ceres's is  $2,161 \text{ kg m}^{-3}$  (R. S. Park et al., 2019). Psyche remains one of the densest asteroids known.

To demonstrate the range of possible compositions consistent with any given bulk density, we adopt a density based upon a recent mass and effective diameter. A recent estimate of Psyche's mass comes from Baer and Chesley (2017), who find a value of  $(22.87 \pm 0.70) \times 10^{18} \text{ kg}$ . In our following calculations of likely bulk density and composition below and considering the prediction capability of the Baer and Chesley (2017) approach against the well-quantified mass estimates of (4) Vesta and (1) Ceres from the Dawn mission, here we adopt a  $1\sigma$  uncertainty that is 2 times larger than their formal error. For the volume, we adopt the effective diameter estimate of Viikinkoski et al. (2018). Using the mass of Baer and Chesley (2017) and the effective diameter estimate of Viikinkoski et al. (2018), the average bulk density of Psyche would be  $3,780 \pm 340 \text{ kg m}^{-3}$  (see Table 2 and Figure 2).

Psyche's bulk density is among the highest of the main belt asteroids and is representative of many of the X- and M-class asteroids that have been measured with good precision (Hanusš et al., 2017). Although many of the X- and M-class asteroids are interpreted to be metal rich based upon their spectra and radar albedos (e.g., Scheeres et al., 2015) and potentially representative of the iron meteorite parent bodies, best estimates of the bulk density of Psyche are surprisingly low in comparison to solid iron-nickel meteoritic metal ( $7,870 \text{ kg m}^{-3}$  for the mineral kamacite; Smyth & McCormick, 1995). Note that meteoritic metal is usually a mixture of kamacite and taenite, which can be slightly denser still ( $8,260 \text{ kg m}^{-3}$ ; Smyth & McCormick, 1995) but in view of the uncertainties in Psyche's bulk density, we simply use kamacite.

Psyche's bulk density is even slightly lower than measured bulk densities of some stony-iron meteorites (such as the pallasites, the mesosiderites, and Steinbach) that lie between about  $4,200$  and  $4,800 \text{ kg m}^{-3}$  (Britt & Consolmagno, 2003). On the other hand, the bulk density of Psyche is at the upper end of the range for the (pore free) grain densities of ordinary chondrites ( $3,200$ – $3,800 \text{ kg m}^{-3}$ ), enstatite chondrites ( $3,100$ – $3,800 \text{ kg m}^{-3}$ ), and most carbonaceous chondrites ( $2,200$ – $3,800 \text{ kg m}^{-3}$ ) (Britt & Consolmagno, 2003; Scheeres et al., 2015), perhaps permissible within the uncertainty of Psyche density measurement but prohibiting significant porosity. The sole exception is the CB chondrite class that contains high metal contents (Flynn et al., 2018). CB chondrites have an average density of  $5,300 \text{ kg m}^{-3}$  (Macke, 2010).

To investigate plausible compositions of Psyche, we interpret its bulk density in terms of mixtures of iron-nickel metal, nonmetal components, and porosity. The nonmetal components may be intimately mixed silicates (as in a pallasite), troilite or other nonsilicate inclusions, or regions of silicates from the Psyche parent body or from later impactors. The greatest unknowns for Psyche's constitution are its porosity and the fraction and composition of its nonmetallic components.

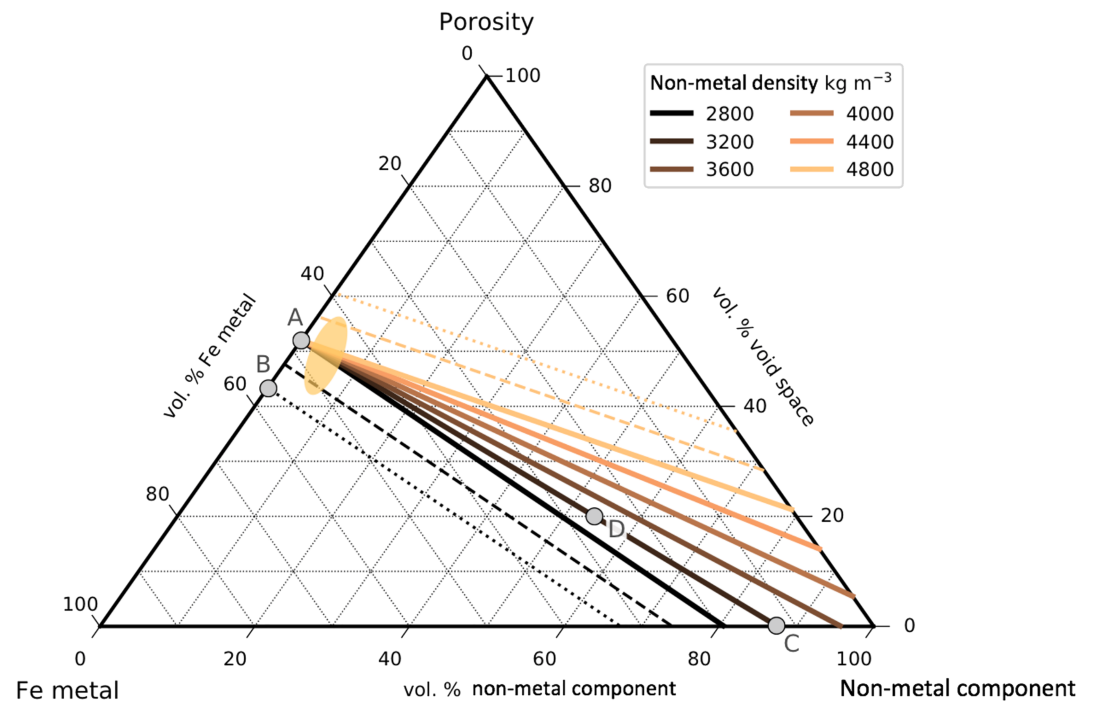


**Figure 3.** Interpretation of the bulk density of Psyche as a mixture of iron-nickel metal, a nonmetal component, and porosity implies that Psyche's metal content may be between ~30 and 55 vol%. The bulk density used is  $3,780 \pm 340 \text{ kg m}^{-3}$ , the density of metal that of kamacite ( $7,870 \text{ kg m}^{-3}$ ), and the density of the nonmetal varied from 2,800 to 4,800  $\text{kg m}^{-3}$  (see text). Each solid line shows the possible makeup using a different nonmetal density, and the dashed and dotted lines show how the results change when using the  $1\sigma$  and  $2\sigma$  limits of the bulk density. The yellow oval marks regions where nonmetals total 10% of the solid, as suggested by remote sensing (see text). At point A, Psyche consists solely of 48% metal and 52% pore space. At the  $2\sigma$  of our density estimate, point B reaches 57% metal and 43% pore space. Point C represents another end-member possibility, where there is no porosity in Psyche, and metal combined with enstatite at  $3,200 \text{ kg m}^{-3}$  implies a maximum of ~13% metal by volume. The addition of 20% porosity increases the abundance of iron metal from 13% to 27% (point D).

Figure 3 plots the allowable volumetric abundances of these three components in the form of a ternary diagram. We use a density of  $7,870 \text{ kg m}^{-3}$  for kamacite, and a range of possible nonmetal compositions:  $4,840 \text{ kg m}^{-3}$  for troilite,  $3,330 \text{ kg m}^{-3}$  for forsterite (Mg-rich olivine),  $3,270 \text{ kg m}^{-3}$  for enstatite (Mg-rich pyroxene), and  $2,770 \text{ kg m}^{-3}$  for anorthite (Bass, 1995; Smyth & McCormick, 1995).

If Psyche consists entirely of metal and pore space with no other material, it must comprise ~48 vol% metal and 52 vol% pore space for a bulk density of  $3,780 \text{ kg m}^{-3}$  (point A in Figure 3) and ~57 vol% metal and ~43 vol% pore space for the  $2\sigma$  upper limit of  $4,460 \text{ kg m}^{-3}$  (shown as point B in Figure 3). If, as another end-member possibility, there is no porosity in Psyche, the best fitting bulk density of  $3,780 \text{ kg m}^{-3}$ , combined with enstatite at  $3,200 \text{ kg m}^{-3}$ , implies a maximum of ~13% metal by volume (point C in Figure 3). The M-type asteroid (21) Lutetia, as a pertinent example, has an estimated bulk density of  $3,400 \pm 300 \text{ kg m}^{-3}$ , and its spectral signature may be a good match with enstatite chondrite meteorites (Vernazza et al., 2011).

Whether Psyche is a whole body or a rubble pile is unknown, equally unknown is the fraction of porosity that can be supported by the strength of metal at the temperatures of Psyche before self-gravity closes the voids. Data from very small bodies indicates that porosity can be maintained throughout the mass: Mass and shape measurements of the asteroids Itokawa and Ryugu imply porosities for these bodies of about 40% (Abe et al., 2006) and >50% (Watanabe et al., 2019), respectively. These bodies, however, are less than a kilometer in diameter. Larger bodies, including Ceres and Vesta, have porosities similar to the lunar crust, implying self-gravitation drives out porosity in silicate and ice bodies.

Gravity data of Earth's Moon, which is significantly more massive than Psyche, implies an average porosity of about 12% for the upper portion of the crust (Wieczorek et al., 2013). In large asteroids the bulk porosity is

less well known but appears to be similar to or even lower than that of the lunar crust. Ceres may have a bulk porosity of 10%–15% (Ermakov et al., 2017). Porosity of the silicate portion of Vesta has also been estimated at 8%–15% with an error of up to 50% (Ermakov et al., 2014) and at 5%–6% (C. T. Russell et al., 2012).

A reasonable bulk porosity for small bodies, based upon the known values listed above, is likely not more than 20%. However, we do not have any authentic knowledge of the ability for metal at the temperatures of Psyche to support pore space. The high strength for iron meteorite material indicated by Marchi et al. (2019) ( $\sim 1,300$  MPa at  $\sim 120$  K) indicates that an iron body may be able to support higher porosity than a silicate rock body could. In the absence of other evidence, we consider a bulk porosity of 20% here. In addition, the experiments of Marchi et al. (2019) display large cracks and interlocking of metallic chunks that increase porosity. Impact brecciation could produce high porosity.

For the case of Psyche with total bulk density of  $3,780 \text{ kg m}^{-3}$  and density of the nonmetal component of  $3,200 \text{ kg m}^{-3}$ , the addition of 20% porosity increases the allowable volumetric abundance of iron metal from 13% to 27% (point D in Figure 3). The range of bulk densities considered in this study also allows a fascinating case where Psyche consists of pure troilite with a porosity between 5 and 20 vol%. A formation process leading to this composition is difficult to envision, and is unprecedented in meteorites, so we consider it highly unlikely

## 2.2. Thermal Inertia

Thermal inertia is a physical parameter that quantifies how quickly the temperature of the surface layer of an astronomical body responds to periodic variations in incident solar radiation (e.g., Spencer et al., 1989). The thermal inertia is defined as  $(k\rho c)^{1/2}$ , where  $k$  is the thermal conductivity,  $\rho$  is the density, and  $c$  is the specific heat capacity. For common meteoritic materials, both the specific heat capacities and densities vary by less than a factor of 3 (Britt & Consolmagno, 2003; Opeil et al., 2012). Their thermal conductivities, however, are highly dependent on porosity and can vary from values as low as  $0.001 \text{ W m}^{-1} \text{ K}^{-1}$  for highly porous materials (e.g., Langseth et al., 1976) to values as high as  $7 \text{ W m}^{-1} \text{ K}^{-1}$  for coherent materials (Opeil et al., 2012).

The thermal radiation emitted by an asteroid depends on the thermal inertia but also its shape, rotation rate, pole orientation, albedo, emissivity, surface roughness, and grain size (see Delbo et al., 2015). For typical asteroid rotation periods, thermal inertia estimates are representative of materials in the upper few centimeters of the surface.

The thermal inertias of almost 200 asteroids have been determined by fitting fluxes derived from thermophysical models to observations (Hanusš et al., 2018). The thermal inertia of an asteroid is found to be broadly correlated with asteroid diameter. Thermal inertias are the highest for asteroids smaller than about 10 km, with values between about 200 and  $800 \text{ J m}^{-2} \text{ s}^{-1/2} \text{ K}^{-1}$ . All cited thermal inertias are here normalized to the temperature conditions experienced at 1 AU, see Delbo et al. (2015). For larger asteroids, values range typically from just under 10 to about  $300 \text{ J m}^{-2} \text{ s}^{-1/2} \text{ K}^{-1}$ .

The most likely interpretation for the transition near 10 km is that the smallest objects do not have their surfaces covered with well-developed fine-grained regolith. Ejecta from impacts is likely a key process for creating fine-grained regolith, but through their exposure ages are generally sufficient for producing a regolith, small bodies may not have the surface gravity requisite for retaining impact ejecta; particles smaller than a mm are susceptible to electrostatic levitation and may eject most smaller grains (e.g., Delbo et al., 2014; Hanuš et al., 2018; Hartzell & Scheeres, 2013; Walsh, 2018).

Thermal inertias appear to be largely independent of the asteroid's spectral class. One possible exception is the M-class asteroids greater than about 10 km in diameter. Though most spectral classes at these diameters span the entire range of thermal inertias, the M-class asteroids are largely confined to the highest values between about 200 and  $300 \text{ J m}^{-2} \text{ s}^{-1/2} \text{ K}^{-1}$ .

The thermal inertia of Psyche, an M-class asteroid, has been investigated by two studies. A value between 243 and  $284 \text{ J m}^{-2} \text{ s}^{-1/2} \text{ K}^{-1}$  was obtained by Matter et al. (2013), which was among the highest measured at that time for large asteroids. They noted that a high iron metal content, as implied by the high radar albedo (discussed below), could give rise to a higher thermal inertia given that the thermal conductivity of iron metal is several times larger than that of silicates. However, in a subsequent study, Landsman et al.

(2018) obtained a considerably lower best-fitting thermal inertia of  $11\text{--}53 \text{ J m}^{-2} \text{ s}^{-1/2} \text{ K}^{-1}$ . This study also obtained a best-fitting bolometric emissivity of 0.9, which is most consistent with the presence of near-surface silicates and little metallic iron.

If the high thermal inertias associated with most M-class asteroids are a result of high iron-metal contents, one might expect to find a correlation between the thermal inertia and radar albedo. Six asteroids have measurements for both the radar albedos from Shepard et al. (2015) and the thermal inertias from Hanuš et al. (2018) (excluding Psyche, whose thermal inertia is debated). We find that two asteroids (Lydia and Edburga) have high radar albedos ( $>0.3$ ) and high thermal inertias ( $>180 \text{ J m}^{-2} \text{ s}^{-1/2} \text{ K}^{-1}$ ), three asteroids have low radar albedos and high thermal inertias (Libera, Kalliope, and Iva), and only one has low values for both (Lutetia). Lutetia is a silicate asteroid, possibly with an enstatite chondrite composition (e.g., Vernazza et al., 2011). These observations suggest that the M-class asteroids are compositionally diverse and that only some of them may be iron-metal rich.

### 2.3. Radar Reflectance

Radar techniques can elucidate several key physical properties of asteroids, including the rotation rate, shape, surface roughness, and radar albedo (e.g., Ostro, 1993). The latter quantity is approximately proportional to the radar reflectivity, which itself depends upon both the composition and porosity of surface materials over meter-scale depths (depending upon wavelength).

The radar albedos of asteroids span a range of more than a factor of 10, from 0.04 to 0.55 (Magri et al., 2007; Shepard et al., 2015; Shepard et al., 2018). The average radar albedos of the common C and S class asteroids are 0.13 and 0.14, respectively, but individual asteroids from both classes range between about 0.04 and 0.26.

The M- and X-class asteroids are exceptional in that some have radar albedos as low as 0.06 and others high as 0.55 (Shepard et al., 2015; Shepard et al., 2018), indicating either considerable variability in composition or porosity of the surface materials of these bodies.

Those asteroids with the highest albedos (greater than about 0.3) are commonly interpreted as being metal rich (e.g., Ostro et al., 1991), but the abundance of metal on these bodies is difficult to quantify remotely. One clue comes from the bulk density of the M-class asteroid (216) Kleopatra, which has one of the highest radar albedos of 0.43. Based on a mass determination from the orbits of natural satellites (Descamps et al., 2011), its bulk density has been determined to be  $4,900 \pm 500 \text{ kg m}^{-3}$  (Shepard et al., 2018), which is considerably less than iron metal but also far more dense than meteoritic silicate rock. Kleopatra must be either a mixture of rock and metal or highly porous metal. Kleopatra has an effective diameter of  $\sim 100 \text{ km}$  and a highly elongated shape which, along with the presence of two small moons, suggests a history that may have involved disruption and reaccretion from a parent body (Descamps et al., 2011). If true, Kleopatra may be a highly porous rubble pile of metal.

Radar observations of Psyche show that its average radar albedo is  $0.37 \pm 0.09$  (Shepard et al., 2017). Of the 29 M- and X-class asteroids investigated by Shepard et al. (2015) only seven have radar albedos as great, making Psyche a prime candidate to be a metal-rich world. The radar albedo, however, is not constant across the surface.

Over the course of its rotation, the disk averaged radar albedo ranges from values as low as 0.25 to values as high as 0.54. The lowest values correspond to the highest measured radar albedos of the S and C class asteroids, whereas the highest values are equaled only by one M-class asteroid, (758) Mancunia (Shepard et al., 2015). The highest values are located over a limited range of subradar longitudes spanning about  $40^\circ$  of rotation, and the lowest values are located approximately on the opposing hemisphere. The simplest interpretation of these observations is that there are significant variations in the metal abundance on the surface of Psyche.

The radar reflectivity depends directly on the average dielectric constant of the surface materials. Silicates have dielectric constants that are about 5 to 10 times greater than free space. The dielectric constants of metals are considerably higher, but when metal contents are high, it is also necessary to consider the effects of electrical currents on the radar reflectivity (Herique et al., 2018).

For a two-component system, where one component is free space from porosity, mixing laws such as the Maxwell-Garnett relation can be used to show that the reflectivity is approximately linear in porosity up

to about 50%. As the density of the solid component is assumed fixed, this is equivalent to having a linear dependence on the bulk density of the material with a fixed grain density.

Empirical relations between bulk density and reflectivity have been used by Shepard et al. (2017) to show that the reflectivity of Psyche could be accounted for by an iron-metal regolith with about 55% porosity. However, the observed reflectivity is also consistent with chondritic materials with zero surface porosity (Ostro et al., 1991). As of yet, there have been no attempts to interpret in a self-consistent manner radar reflectivities in terms of mixtures of silicates, metal, and porosity.

#### 2.4. Optical Reflectance

For the past several decades, asteroids have been classified by their optical and reflectance properties. They have been organized into taxonomies suggestive of possible surface compositions (e.g., Tholen, 1984). Tholen separated the X-types into the E, M, and P types based on their visual wavelength albedos. In Tholen's taxonomy, Psyche was characterized as an M-type asteroid, a subclass of the larger X-type asteroid class. The X-type asteroids have relatively featureless, red-sloped (increased reflectance with increased wavelength) spectra at visible to near-infrared wavelengths, consistent with metallic surfaces.

Over the next several decades, advances in telescopic observing equipment allowed higher-resolution reflectance data to be collected at a wider wavelength range, enabling novel classification of asteroids and identification of previously unknown spectral details (Burbine & Binzel, 2002; Bus & Binzel, 2002; DeMeo et al., 2009). In the Bus-Binzel-DeMeo classification system, Psyche is categorized as an Xk type, meaning its spectrum from  $\sim 0.4$  to  $2.5 \mu\text{m}$  is "slightly curved and concave downward but with a faint feature between 0.8 and 1 micron." (DeMeo et al., 2009).

Alongside asteroid observation work are efforts to collect spectral data of minerals and meteorites. Meteorite and mineral spectra provide constraints on the possible surface compositions of M-type asteroids based on the presence or absence of characteristic absorption features (e.g., Gaffey, 1976). Many authors sought to explain how variations in surface roughness, mixtures of minerals or meteorite types, and optical properties like phase angle and polarization play a role in our interpretation of the collected asteroid spectral data (e.g., Britt & Pieters, 1988; Cloutis et al., 1990a, 1990b; Dollfus et al., 1979; Lupishko & Belskaya, 1989).

Broadly speaking, much of this work points toward Psyche having a surface that is dominated by relatively fine-grained ( $20\text{--}50 \mu\text{m}$  in size) iron-nickel metal but with a significant component of low-Fe, low-Ca orthopyroxene. Note that there is little understanding of how a regolith may be formed from iron meteoritic material; forthcoming work on solar wind and impact effects may aid in this understanding.

Subsequent efforts to collect spectral data specifically of M- and X-type asteroids supported the interpretation of a low abundance of low-Fe, low-Ca orthopyroxene mixed with metal on the surface of Psyche (e.g., Clark et al., 2004). Multiple surveys of M-type asteroids (e.g., Hardersen et al., 2005; Ockert-Bell et al., 2010) report that the  $0.9\text{-}\mu\text{m}$  feature is ubiquitous over several of Psyche's rotation periods. This has been interpreted as an indication that the pyroxene component is intimately mixed with other materials across most of the asteroid's surface. Sanchez et al. (2017) also studied the  $0.9\text{-}\mu\text{m}$  feature (and its variability across Psyche) and concluded that the surface has an average orthopyroxene content of  $6\% \pm 1\%$ .

If Psyche is a disrupted planetary core, it may be possible for mafic mantle material to have reaccumulated on the surface, some of which could be olivine. Pure magnesium olivine (forsterite) has a featureless, red-sloped spectrum (e.g., Adams, 1975) but has a much higher overall reflectance than what is measured for Psyche ( $>70\%$  at  $0.55 \mu\text{m}$  compared to  $\sim 12\%$  for Psyche). With even 2–5 mol. % fayalite substituted in the olivine composition, a  $\sim 1.03\text{-}\mu\text{m}$  feature is apparent in the spectrum (Hunt & Salisbury, 1970; Sunshine & Pieters, 1998). As the olivine composition becomes more Fe-rich, this absorption feature increases in depth and becomes multilobed (Adams, 1975). This feature is not observed in any published spectra of Psyche. Olivine compositions in pallasite meteorites range between  $\sim 10$  and 20 mol.% fayalite and is often at centimeter or larger grain sizes (Buseck, 1977). This material should be easily measured by terrestrial observatories as a  $>1\%$  deep absorption feature centered longward of  $1.03 \mu\text{m}$  if the olivine grain size has remained above  $45 \mu\text{m}$  in size (Cloutis et al., 2009). Because no features at wavelengths longer than  $1.0 \mu\text{m}$  have been observed in the spectrum of Psyche, it is unlikely that olivine as seen in pallasites exists on the surface.



Observations of a shallow absorption feature at  $0.43\ \mu\text{m}$  in the spectrum of Psyche presented evidence that the asteroid's surface composition is not fully described by metal and pyroxene (Fornasier et al., 2010). This absorption feature could be attributed to either clinopyroxene minerals, the iron sulfate mineral jarosite, or chlorite and Mg-rich serpentine. If the latter was true, could the surface of Psyche also carry significant amounts of hydrated minerals? Initial observations of hydration features at  $3\ \mu\text{m}$  in the spectra of M-type asteroids did not indicate that Psyche is significantly hydrated (Rivkin et al., 1995; Rivkin et al., 2000), although recent work has reported a shallow and rotationally heterogeneous absorption feature in this wavelength range (Takir et al., 2016). The presence of these features is interpreted by the Psyche science team and others to be the remnants of infall of carbonaceous material over the age of the surface, perhaps as long as the past 4.5 Gyr, similar to what was detected at the asteroid Vesta (Prettyman et al., 2012).

Rotationally resolved spectra of Psyche did not originally indicate a significant variation in the surface composition; however, these observations were restricted to the visible and near-infrared spectrum between  $0.50$  and  $0.9\ \mu\text{m}$  (Binzel et al., 1995). Further observations up to  $\sim 2.5\ \mu\text{m}$  indicated that while the depth of the  $0.9\ \mu\text{m}$  band did not change over Psyche's rotation period, the overall slope varied significantly (Ockert-Bell et al., 2010). More recent observations covering a larger range of Psyche's surface indicate variation of the depth of the  $0.9\text{-}\mu\text{m}$  absorption feature and, therefore, may represent varying abundances or chemistry of the purported pyroxene component on the asteroid's surface (Sanchez et al., 2017).

Predictions of silicate fraction on the surface are derived from matching spectral investigations of the asteroid with detailed spectroscopic studies of iron-silicate mixtures. The reported band depths for Psyche's  $0.9\text{-}\mu\text{m}$  feature range from  $\sim 0\%$  (Ockert-Bell et al., 2010) up to  $2.9\%$  (Fornasier et al., 2010). This band depth corresponds to intimate mixtures of metal and  $<20\ \text{wt.}\%$  orthopyroxene, both of a grain size  $<45\ \mu\text{m}$  (Cloutis et al., 2009). However, we note that the reported band centers of these mixtures ( $0.915\text{--}0.917\ \mu\text{m}$ ) are on the short edge of reported band centers for Psyche ( $0.919\text{--}0.950\ \mu\text{m}$ ) (Cloutis et al., 2009; Fornasier et al., 2010; Hardersen et al., 2011; Ockert-Bell et al., 2010; Sanchez et al., 2017), which may result from a difference in pyroxene chemistry or an additional mineral component on the surface. More conservative interpretations of Psyche's reflectance spectrum include a mixture of  $90\ \text{wt.}\%$  metal and  $10\ \text{wt.}\%$  orthopyroxene (Hardersen et al., 2011), only  $6\ \text{wt.}\%$  orthopyroxene (Sanchez et al., 2017), and even a strictly metal powder (Fornasier et al., 2010). A possible set of compositions consistent with around  $10\%$  nonmetal and  $90\%$  metal with varying porosity is shown by the yellow oval in Figure 3.

The CB chondrites are another group of meteorites that have been discussed as potential surface analogs of Psyche (e.g., Hardersen et al., 2011). Their high metal abundance ( $60\text{--}80\ \text{vol.}\%$ ) and low-iron silicates are consistent with general models of Psyche's surface composition. Spectra of CB chondrites are typically relatively featureless and red sloped, with minor absorption features between  $0\%$  and  $3\%$  at  $0.9\text{--}1.1\ \mu\text{m}$  (e.g., Cloutis et al., 2018; Trigo-Rodríguez et al., 2013). Hardersen et al. (2011) discount CH/CB chondrites as potential surface analogs for Psyche since they reported an absorption band center for the asteroid  $>0.94\ \mu\text{m}$ . However, since the range of reported band centers for Psyche now spans from  $0.919$  to  $0.950\ \mu\text{m}$ , the CB chondrite interpretation may still be valid.

Within the last few years, observations of Psyche in the ultraviolet and midinfrared have proved enigmatic. Using the Hubble Space Telescope's Space Telescope Imaging Spectrometer, Becker et al. (2017) concluded that Psyche's UV spectrum between  $0.16$  and  $0.3\ \mu\text{m}$  is inconsistent with significant amounts of pyroxene on the surface. Conversely, Spitzer Space Telescope data in the midinfrared ( $5\text{--}14\ \mu\text{m}$ ) is interpreted by (Landsman et al., 2018) to indicate that Psyche likely has smooth metallic bedrock with fine-grained ( $<75\ \mu\text{m}$  in grain size) silicates intermixed with iron grains.

The relatively featureless nature of Psyche's spectra makes tempting the conclusion that it has a largely metal surface, and indeed, it may have. But similarly, no silicate features were observed in spectra for Lutetia, which has been revealed by Rosetta mission data as having an entirely silicate surface (Coradini et al., 2011). The MASCS instrument on the MESSENGER mission recorded a flat spectrum free of silicate absorption features for Mercury, and Mercury has a low-iron silicate ( $<2\ \text{wt.}\%$ ) surface (Domingue et al., 2010; McClintock et al., 2008). Thus, importantly, the relative featurelessness of its spectra cannot alone be an indicator for a metallic surface: such spectra have nonunique interpretations.

### 2.5. Summary of Earth-Based Observations of Psyche

Psyche's bulk density appears to be in the vicinity of  $4,000 \text{ kg m}^{-3}$  based upon a number of recent observations and between  $3,400$  and  $4,100 \text{ kg m}^{-3}$  from the analysis of the authors (see Table 2). To further constrain Psyche's composition, observations beyond density, such as radar albedo, reflectance spectra, and thermal inertia, must be considered. The reflectance and optical properties of Psyche indicate nonuniquely that the body may be largely metallic; the interpretation of a partial metal surface is supported by measurements of the body's density and radar albedo. Another major component may be a low-Fe, low-Ca pyroxene. These materials are likely heavily fractured and fine-grained. Impacts with asteroidal or cometary bodies probably have left large concentrations of exogenous, perhaps hydrated, carbonaceous material randomly distributed on the surface. These contributions may be correlated with craters, or they may coat the oldest surfaces as a result of continuous infall.

Given the data currently available for Psyche, and its interpretations as given above, Psyche is predicted to have between  $\sim 25$  vol% metal (point D in Figure 3) and  $\sim 60$  vol% metal (the high-metal end of the yellow oval in Figure 3). Point D marks  $\sim 25$  vol% metal,  $\sim 55$  vol% nonmetal component with density consistent with magnesian pyroxene, and  $\sim 20$ % pore space.

## 3. Meteorites as Analogs to Psyche

The compositions and physical characteristics of a hand-sample-size meteorite cannot necessarily be extrapolated to the scale of Psyche. Nevertheless, discussion of similarities and differences of Psyche observations to those expected of meteoritic materials can help constrain models and interpretation of eventual spacecraft data. In particular, comparisons of orbital geochemistry data with meteoritic and returned sample data have provided useful information for studies of the asteroids Vesta and (433) Eros (Beck et al., 2015; Beck et al., 2017; Peplowski et al., 2015) and the Moon (Peplowski et al., 2016).

Among the most robust ground-based constraints available from Psyche for comparison to meteorites are the density and possible presence of relatively magnesian mafic silicates. Density provides a more stringent test, given that numerous mechanisms can reduce the bulk density of an asteroid, including formation of both microporosity and macroporosity, but no obvious mechanisms exist to increase the bulk density of an asteroid from that of its components.

With the recent determination of the density of Psyche perhaps as low as  $3,440 \text{ kg m}^{-3}$  (the  $1\sigma$  lower bound on the density estimate from this paper), a range of possible meteorite analogs for Psyche become permissible, including iron meteorites with densities in the  $7,000$  to  $8,000 \text{ kg m}^{-3}$  range; pallasites with densities ranging from  $4,100$  to  $7,800 \text{ kg m}^{-3}$ , dependent on the ratio of silicate to metal; mesosiderites with densities from  $3,100$  to  $7,200 \text{ kg m}^{-3}$ , depending on the ratio of silicate to metal; and CB chondrites, with an average density of  $5,300 \text{ kg m}^{-3}$  (Macke, 2010). Some enstatite chondrites range up to  $3,800 \text{ kg m}^{-3}$ , perhaps permissible without porosity given the uncertainty of the Psyche density measurement.

### 3.1. Iron Meteorites

Iron meteorites, defined by their high proportion of iron-nickel metal, include at least 13 distinct compositional groups, each from a distinct parent asteroid and represented by at least five samples from that parent body. More than 50 additional planetesimals or asteroids may be represented by the  $\sim 15$ % of iron meteorites that do not fall into these well-defined groups and thus are termed ungrouped (Wasson, 1990; Weisberg et al., 2006). Some features that vary between the groups may relate to measurements to be made from orbit around Psyche: major element chemical composition, light elements (e.g., S, C, P, and Si), abundance, mineralogy, mineral compositions of silicates, and the presence or absence of a detected paleomagnetic field. A few examples suffice to illustrate these points.

Iron meteorites differ significantly in their Fe/Ni ratio, primarily as a result of oxidation. A higher level of oxidation means more iron will be included in silicates in the form of FeO, while greater reduction will move  $\text{Fe}^0$  into the core during differentiation. Oxidation state may also be reflected in the presence of reduced phases of carbon (graphite or the iron carbide cohenite), phosphorus (the Ni-phosphide schreibersite), sulfur (the Cr-bearing sulfide daubréelite), and rarely, silicides such as perryite in the most reduced, Ni-poor

meteorites. Their oxidized equivalents, phosphates, chromite, and tridymite ( $\text{SiO}_2$ ) are observed in the most oxidized, Ni-rich meteorites.

Troilite is ubiquitous in iron meteorites, but tends to be more abundant in the lower-Ni irons. Rare silicates are found in many groups of iron meteorites, but silicates are more abundant in the IAB, IIE, and IVA irons. Notably, silicates in the IAB and IVA irons tends to be dominated by relatively magnesian olivine and pyroxene. The composition of olivine in IAB irons is typically  $\text{Fa}_{3-8}$  and orthopyroxene  $\text{Fs}_{7-9}$  (Bunch et al., 1970). IVA irons contain pyroxenes of  $\text{Fs}_{14-15}$  with tridymite (Scott et al., 1996). The IIE irons contain orthopyroxenes of more iron-rich compositions, with the range  $\text{Fs}_{14-23}$ .

In the context of these groups, silicate-free irons are more prevalent than silicate-rich irons, likely suggesting that if Psyche were composed of iron meteorites, a low bulk density would require substantial macroporosity. Interestingly, some silicate-bearing IVA and IIE irons record paleomagnetic evidence of an ancient dynamo on their parent bodies (Bryson et al., 2017; Maurel et al., 2019), matching the primary hypothesis for Psyche's formation as core material from a differentiated planetesimal.

Pallasites, with a density approximating that of Psyche, are mixtures of iron-nickel metal and olivine or pyroxene. Pallasites are composed of Fe,Ni metal with an average Ni concentration of ~9–12 wt.%, mixed with olivine of  $\text{Fa}_{11-20}$ . Olivine makes up an average of 65 vol% of pallasites (Buseck, 1977). Although most pallasites belong to the so-called “main group,” based on their distinct oxygen isotopic signatures, pallasites likely sample a number of parent bodies. The pyroxene pallasites, Eagle Station, and the Milton pallasite likely represent different parent bodies. For the sake of brevity, we limit our discussion to main group pallasites.

In the traditional view, pallasites formed at the core-mantle boundary of an asteroid and any intact asteroidal core dominated by a pallasitic surface would be expected to overlie a denser metallic center. Cooling rates of main group pallasites vary by a factor of 4 (Yang et al., 2010). Though Yang et al. (2010) claim that such a range of cooling rates are inconsistent with formation at the core-mantle boundary, we disagree: Planetesimals were likely being stripped or added to, constantly, and thus, a wide range of cooling rates is expected even for the core-mantle boundary of a planetesimal.

Yang et al. (2010) suggested that pallasites formed from hit-and-run collisions of the type envisioned by Asphaug et al. (2006). Yang et al. (2010) proposed that the hit-and-run collision can result in the formation of a secondary body dominated by the mantle of the primary body with interspersed molten metal. If formed in such a way, the mixture of silicates and metal could be constant throughout the body, or it may vary unpredictably.

Mesosiderites are mixtures of basaltic and orthopyroxenitic crustal or mantle material mixed with metal. The broadly accepted though complex history begins with formation of a differentiated planetesimal that was similar in many respects to Vesta (parent body of the howardite-eucrite-diogenite meteorites) but distinct in mineralogy and chemistry (Mittlefehldt et al., 1998). This differentiated parent body collided with a metallic core, perhaps, while still molten, produced metal-silicate mixing. Rapid cooling at high temperatures was followed at about 4.2 Ga by breakup and reassembly that allowed slow cooling recorded in the metal.

With bulk densities within the range of Psyche, mesosiderites are a permissible analog from this perspective. There are, however, several objections to a link between mesosiderites and Psyche, notably that mesosiderites are not expected to constitute the dominant lithology on their parent asteroid and, more importantly, that mesosiderites, like HEDs, have remarkably FeO-rich silicates ( $\text{Fs}_{14-50}$  in pyroxene) (Mittlefehldt et al., 1998). Thus, one would expect reflectance spectra of a mesosiderite lithology to be similar to that of Vesta, the likely parent body of the HEDs, quite in contrast to observations of Psyche.

### 3.2. Chondrites

In contrast to all of the meteorites discussed above, CB chondrites, with an average density slightly greater than that of Psyche, originate not from a melted, differentiated planetesimal, but from a primitive chondritic parent body or from the pristine lid of a partially differentiated planetesimal. The CB meteorites are comprised of ~60 vol% metal (Krot et al., 2005) The remainder of the CB materials is either millimetric or centimetric chondrules that exclusively have skeletal olivine and cryptocrystalline textures, and the group is

divided into the CBa and CBb meteorites based on chondrule size. The origins of CB chondrites have been highly debated and hypotheses include both nebular and parent body impact scenarios (Krot et al., 2005). Silicates within the chondrules are highly magnesian, with olivine of  $Fa_{2-4}$  and pyroxene of  $Fs_2$ . The metal in CB chondrites typically has less than 8 wt.% Ni (Brearley & Jones, 1998).

The scale of metal regions within the silicate of chondrites can also vary. Shock melting or radiogenic partial melting could produce veins of metals on a larger scale, as are seen in Portales Valley (Kring et al., 1999).

### 3.3. Summary of Meteorite Comparisons With Psyche

Pallasites (likely pyroxene-rich rather than olivine) and CB chondrites can match both Psyche's density and the presumably high-magnesian composition of its silicates. Though their density is equivalent, mesosiderites are an unlikely analog to bulk Psyche, both because the parent body of the mesosiderites is not expected to be pure mesosiderite and because mesosiderites have far more iron-rich silicates than Psyche appears to have.

Using density as a determiner, Psyche (presumed density between 3,400 and 4,100  $\text{kg m}^{-3}$  from the  $1\sigma$  error bounds on the estimate from this paper) could consist of pallasitic material (some with density around 4,100  $\text{kg m}^{-3}$ ) throughout. This case requires that pallasites formed as a relatively homogeneous mixture of low-iron pyroxene and metal via a hit-and-run collision between far larger bodies that simply spalls off a secondary body (Psyche), itself a mantle-core mixture.

If, alternatively, pallasites are a veneer over a relatively intact iron-nickel metal core, such a body would require high porosity to match Psyche's density. Such a high bulk porosity remains a possibility.

CB chondrites have appropriate density and magnesian silicates. If Psyche has remanent magnetization and matches the CB chondrites compositionally, then the parent body was likely either a fully differentiated body which then mixed with something chondritic, or it was a partially differentiated body with a chondritic crust.

## 4. Planetesimal Formation and Evolution Scenarios

A fundamental goal of the Psyche mission is to understand the formation of the asteroid Psyche and to tie its formation to the formation of our Solar System. Armed with the understanding, from radiogenic dates and decades of prior research, that the asteroid belt contains the remnants, the scraps, of planet formation, Psyche should ultimately be placed in the context of planetesimal formation, accretion, and destruction.

Planetesimals of hundreds or thousands of kilometers in diameter form very rapidly after the formation of the first millimeter- or centimeter-sized condensates in our solar system (the calcium-aluminum inclusions, or CAIs, dated to 4.568 Ga by Connelly et al., 2008). Age models based on radiogenic isotopes show that iron meteorites formed within just 500,000 years of CAIs (Scherstén et al., 2006). Models of pebble accretion, by which millimeter- and centimeter-sized objects are slowed by gas drag and efficiently accreted by the gravitational fields of growing planetesimals, show that the radii of planetesimals under this process can double in  $10^3$  years (Ormel & Klahr, 2010).

Planetesimals, the building blocks of the terrestrial planets and presumably the parent bodies of both asteroids and through them meteorites, were heated by the short-lived radioisotope  $^{26}\text{Al}$  (Fish et al., 1960; Urey, 1955). The extent and degree of heating depends upon the time of accretion relative to the time of nucleosynthetic origin of the  $^{26}\text{Al}$ , the amount of ice in the accreting material, and possibly upon varying concentrations of initial  $^{26}\text{Al}$ . Judging from meteorites, some planetesimals gently heated and experienced fluid fluxes but did not melt. Others may have melted partially from the interior but retained a primitive (chondritic) lid (Elkins Tanton et al., 2011). Still others appear to have melted entirely. For a thorough review of planetesimal processes, see B. P. Weiss and Elkins Tanton (2013).

### 4.1. Psyche as a Remnant or Mixture of Differentiated Parents

The simplest process by which to imagine creating concentrated metal is via melting and differentiation of a planetesimal to form a metal core. If a fully differentiated parent planetesimal was then stripped of its rocky exterior in a series of hit-and-run impacts, then Psyche may be the stripped core of a planetesimal (Yang et al., 2007). In that case, its exterior may have sheets of its parental rock, fallen back after stripping, and

as in all cases it will likely have minor chondritic material from subsequent impacts. In fact, the possible forms of silicate material delivered and processed by impacts have recently been added to by the discovery of glasses and foams from silicate impactors onto metal in laboratory experiments (Libourel et al., 2019).

If Psyche is the greater part of a planetesimal core, then its density as known now probably prevents it from being an intact metal core. An intact iron-nickel metal core would have nearly twice the density of Psyche, as summarized in this paper. However, the density requirement is achieved if Psyche is either a rubble pile with significant porosity, or if it retains 25 to 80 km of silicate rock on its surface (Johnson et al., 2019), or if it is greatly enriched in sulfur. Having a fully silicate surface is likely precluded by the radar reflectance data, which implies that the interior is also at least partially metallic.

Sulfur, however, remains an enigmatic component of planetesimal core formation. Chabot (2004) and Goldstein et al. (2009) find that to explain their trace element profiles iron meteorites must have formed in the presence of significantly higher sulfur content than is now found in the form of troilite inclusions in meteorites. Further, when in molten form with iron and nickel, sulfur segregates into an immiscible liquid when its concentration reaches about 5 wt% (Goldstein et al., 2009; Jones & Drake, 1983). Could this sulfur-rich liquid have been trapped inside of the solidifying core and remain there today as a low-density inner core? Could it have erupted onto the surface of Psyche and be seen as troilite-rich flows?

Using average bulk chondrite compositions and assuming all iron metal and sulfur melt eutectically and mix into a differentiated core, the liquid metallic core may start with between 11 wt% (H chondrites) and almost 60 wt% (CO and CV chondrites) sulfur (Bercovici et al., 2019; Jarosewich, 1990). Perhaps, Psyche will add information to the mystery of the missing sulfur from planetesimal cores.

If a magma ocean on a planetesimal fractionally solidifies, there is only a small window of opportunity for olivines to settle to the core-mantle boundary before high crystallinity prevents any further segregation. Note that olivines are almost invariably the first-crystallizing minerals for all chondritic bulk compositions; see Elkins-Tanton (2016) for phase diagrams and discussion. This is a critical argument for all models for pallasite formation: Their formation needs to exclude other minerals. And once in contact with a highly reducing iron core, especially if the mantle has been stripped by impacts, these olivines may be reduced to pyroxenes. If Psyche is found to consist mainly of iron-nickel metal and pyroxenes, the reduction of olivine from an originally pallasitic bulk composition is a strong contender for a model for its formation.

The observation that Psyche may have significant surface silicates can be satisfied with either inefficient stripping of the silicate exterior of the parent body or by creating Psyche by mixing compositions from much larger initial bodies. The mixture must include the high-magnesian silicates found preferentially at the core-mantle boundary and exclude the more iron-rich materials perhaps found in shallow magma chambers or second-stage eruptive products, hence the requirement of much larger impacting planetesimals, to provide the necessary volume of metal plus high-magnesian material, while excluding other silicates. On smaller bodies, the volume of core plus the very bottom of the silicate mantle (the high-Mg portion) would not be sufficient to make a body Psyche's size.

The scenarios above mainly produce a metal body, perhaps mixed with low-iron silicate on a grain scale (the pyroxene pallasite model), with sulfur-rich material inside or erupted onto the outside and with a varying thickness of primordial, magnesian mantle silicates on its surface. If, however, Psyche is a rubble pile (or was a rubble pile now sintered or cold welded) of blocks of silicate and metal, then the modeling of its formation becomes even more complex and interesting. The physics of mixing pieces of metal and rock above a grain scale presents a complex problem.

#### 4.2. Psyche as Unmelted, Undifferentiated Material

Beyond being a core fragment or otherwise a core remnant mixed with silicates, Psyche may consist of primitive, unmelted, and undifferentiated material like the chondrites. The CB chondrites appear to fit all currently measured Psyche parameters and may be themselves a mixture of a chondritic and a differentiated impactor.

A further possibility exists: Psyche may consist of unmelted primitive material so reduced that its iron is overwhelmingly in the form of metal. Weidenschilling (1978) proposed that Mercury might have formed of highly reduced material sorted via drag, explaining its large metal fraction, now expressed by an

outsized core. To take the concept a step further, the far smaller Psyche may have been formed by highly reduced material near the young Sun, accreted as pebbles, and never melted. We do not know and may never know, where in the solar system Psyche originally formed.

## 5. Discriminating Among Formation Scenarios Using Psyche Spacecraft Instrumentation

The Psyche spacecraft will carry a magnetometer, redundant multispectral imagers, and a gamma-ray and neutron spectrometer. We will also conduct gravity science using the X-band high gain antenna and the three low gain antennas.

If Psyche's silicates originate from the mantle of a differentiated parent body, the material may be mixed with metal on the grain scale (think of a pallasite hand sample) or may exist as sheets many kilometers across that fell back to the surface after the stripping impacts. If, on the other hand, Psyche's silicates formed simultaneously with its metals as primitive chondritic materials, they will be intimately mixed on a grain-scale (though there may well be large-scale structures as well).

### 5.1. Imaging and Spectroscopy

Each imager is equipped with one wide-band panchromatic filter (referred to later as the “clear” filter) and seven narrow-band filters tuned to the science objectives of the mission. The imagers will determine the smallest scale at which the mission data can discriminate silicate and metal material. If the mixing is below imager resolution, the metals and silicates are considered intimately mixed, likely on a grain scale. The imager's pixel scale will vary from several dozen meters per pixel at the spacecraft's highest orbit down to several meters per pixel in the lowest orbit. If observed, the depth and width of a  $\sim 1.0\text{-}\mu\text{m}$  absorption feature can be used to assess the abundance and mixing of silicate components on the surface.

The gamma-ray and neutron spectrometer will measure the abundances of H, Fe, Ni, Si, K, S, Al, Ca, Th, and U in Psyche's surface and near subsurface. A primary gamma-ray and neutron spectrometer measurement is quantifying Psyche's Fe and Ni content. Ni is a key indicator of whether Psyche is a core or unmelted material. Based on models of core formation, if we find more than 4 wt% Ni we can infer that Psyche is a core. For silicates, the elemental measurement will be sufficient to determine whether large areas of silicates are chondrites or achondrites (Figure 4).

Orbital geochemistry investigations using nuclear spectroscopy typically make measurements of surface composition at scales  $>10$  km, which contrasts sharply with meteorite samples at a centimetric spatial scale. Moreover, meteorite composition is typically measured at the grain scale. Thus, a large number of meteorite composition measurements, appropriately selected and scaled, are required to provide elemental composition at a representative scale for comparison to orbital geochemistry data (Beck et al., 2015; Nittler et al., 2004; Usui & McSween, 2007). Regolith breccias may be most representative as they have been thoroughly mixed by impacts, which sample larger spatial scales (Prettyman et al., 2006).

Despite these challenges, multiple studies have successfully compared orbital compositional measurements with meteoritic compositions. For example, gamma-ray and neutron data from NASA's Dawn mission conclusively linked the elemental composition of the asteroid Vesta with that of the Howardite, Eucrite, and Diogenite meteorites (e.g., Beck et al., 2015; Prettyman et al., 2012). Gamma-ray data from NASA's NEAR mission provided robust evidence that the elemental composition of the asteroid Eros is consistent with the L and LL ordinary chondrites (Peplowski et al., 2015), consistent with near-infrared spectral data and forming a robust link between Eros and the L and LL chondrites. On the Moon, thermal neutron data were compared with meteoritic and returned sample data to map locations of nearly pure anorthosite in the lunar highlands (Peplowski et al., 2016).

Thus, meteorite composition data can be comparable to asteroid measurements when proper meteorite databases that represent whole-rock compositions are available for reference. This is particularly true for objects with uniform composition (e.g., Eros) or objects with well-developed regoliths whose composition is represented by regolith breccias (e.g., the howardites and asteroid Vesta or the lunar highlands). Multispectral imaging provides valuable context for the orbital geochemistry measurements, as it often provides an indication of chemical variability at a spatial scale well below that of the geochemical data, and closer to that of the meteoritic analogs.

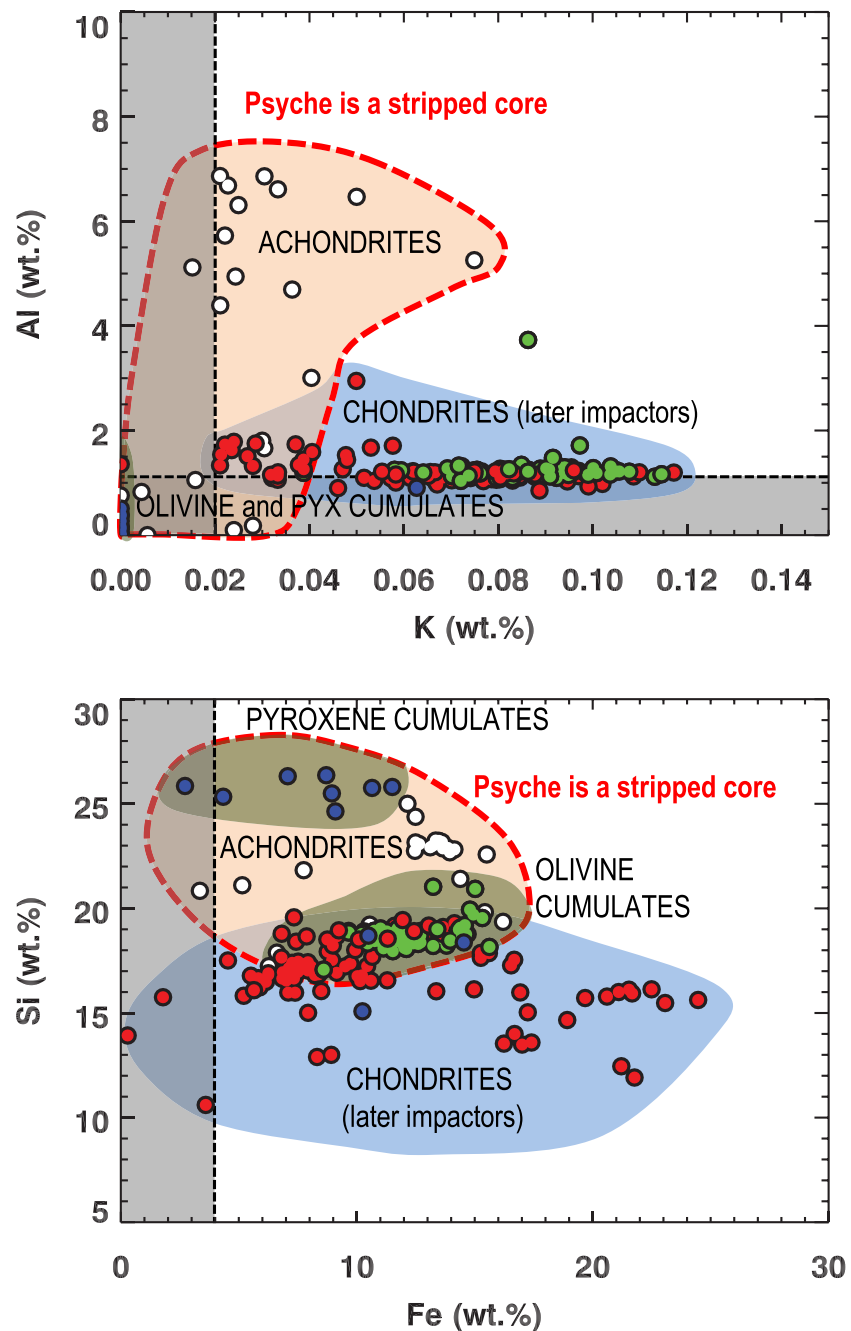


**Figure 4.** The elemental compositions of silicates that may be detected on Psyche can be used via GRNS data to constrain formation models for Psyche. Pyroxenes and olivines dominating a region are assumed to be cumulate material from solidification of a planetesimal magma ocean. Therefore, they would likely be from Psyche's parent body's mantle and, thus, indicate that Psyche is the remnants of a differentiated planetesimal. Extensive achondritic material would be assumed to be the bulk silicate mantle or lid from Psyche's parent body, fallen back during stripping impacts, and also therefore indicate that Psyche is the remnants of a differentiated planetesimal. Chondritic material lying atop metal, in contrast, would likely be accreted by later impacts and therefore would not be indicative of Psyche's formation process. The grey bands block compositions below the detection limit of Psyche instruments. Chondrite and achondrite compositional data from Jarosewich (1990); pyroxene and olivine from pallasites and IIE irons from Mittlefehldt et al. (1998); orthopyroxenes from Steinbach meteorite from Scott et al. (1996). In addition to the natural materials, the olivine cumulate data in the Si versus Fe figure also includes compositions of modeled olivines each calculated as the first-solidifying phase with Fe-Mg  $K_D$  of 0.32 from a hypothetical bulk silicate magma ocean composed of the total oxides of a chondrite measured by Jarosewich (1990).

## 5.2. Magnetometer Investigations

The magnetometer consists of two sensors mounted on a fixed 2-m boom in a gradiometer configuration. The magnetometry investigation tests the hypothesis that Psyche is a core by looking for evidence of a remanent magnetic field generated as the core crystallized starting at the outside and moving inward.

A dynamo is the process by which motion of a conducting fluid inductively generates a magnetic field. In differentiated terrestrial planetary bodies, the dynamo process operates in the metallic core, whose motion is commonly powered by planetary cooling (convection). Although asteroids were largely frozen by 500 Myr after solar system formation, many older planetesimals were molten and apparently generated dynamo magnetic fields (Scheinberg et al., 2017; B.P. Weiss et al., 2010). In particular, Bryson et al. (2017) demonstrated that the parent body of the IVA iron meteorites, thought to be a mantle-stripped planetesimal, generated a dynamo magnetic field that was recorded as remanent magnetization inwardly cooling metallic crust. Thus, a key discriminator between the hypotheses that Psyche is a mantle-stripped planetesimal versus that of an unmelted, iron-rich body would be the identification of remanent magnetization from orbital magnetic field observations from the Psyche spacecraft.

Because the existence of substantial magnetization would strongly indicate that Psyche was a mantle-stripped planetesimal, a key goal of the Psyche mission is to measure the magnetic field intensity and direction around asteroid Psyche. In an inwardly crystallizing body, the interior could be molten and generating a field while the outer portion of the body could cool below the Curie temperature, the critical temperature at which remanent magnetization would be acquired. In particular, thermal evolution models suggest that the outer few tens of kilometer of the IVA meteorite parent body could have cooled below the 780 °C Curie temperature of the Fe-Ni mineral kamacite while the interior was still molten and convecting. By comparison, the absence of strong magnetization would be indeterminate because there are many scenarios in which Psyche could have been a molten, mantle-stripped body but not self-magnetized. For example, a molten Psyche may not have generated a dynamo, or perhaps, it did generate one but crystallized from the inside out, such that the solid portion of the body was always above the Curie temperature.

Based on remanent magnetization measured in iron meteorites, our models predict fields from as low as 0.2 nT to as much as 38,000 nT in the unlikely case that the body is uniformly magnetized (Oran et al., 2018). Measurement of magnetic fields over many orbits allows detection of Psyche's dipole moment for the weakest potential fields even at the highest orbital altitudes. If a remanent field is measured from Psyche, then Psyche originated as material on a body that had a core dynamo: That is, Psyche is part of a differentiated planetesimal.

The magnetometers will further be used to investigate interior structure and compositions. Electromagnetic sounding is a technique used to study the internal structure of solid bodies using their response to natural or artificial external magnetic fields. Variations in the external field induce electrical eddy currents within the body, which in turn generate a secondary magnetic field that can potentially be detected on the surface or by spacecraft (Olsen, 1999).

The inductive response strongly depends on the electrical conductivity distribution within the body. Electromagnetic sounding methods use magnetic field measurements to reconstruct the internal conductivity, which itself depends on the physical, mineralogical, and the thermal properties of the planetary material (Verhoeven et al., 2005). Electromagnetic sounding can therefore complement other types of geophysical data, such as gravity measurements and spectroscopy, and can assist in placing constraints on their internal structure and evolution. Magnetic field data gathered by spacecraft were used to obtain the electrical conductivity within the body for the Earth (Olsen, 1999), the Moon (Hood et al., 1999; C.T. Russell et al., 1981), and Europa (Khurana et al., 2009).

The Psyche mission and the magnetometer experiment will collect a high volume of magnetic field data under varying conditions of the interplanetary magnetic field. Since the interplanetary magnetic field is carried by the variable and turbulent solar wind, Psyche will be subjected to magnetic field variations that can be used in sounding, such as sharp changes in the field direction, and electromagnetic waves. These data can be proceeded to determine the interior conductivity profile of Psyche (Dyal & Parkin, 1973; Khurana et al., 2009), subject to the limiting skin depths of different signals. Such a conductivity profile can potentially constrain the metal content and porosity as a function of depth.



It is not yet known whether Psyche has an internal magnetic field. This presents two different scenarios for electromagnetic sounding of Psyche's interior: one for a nonmagnetized conductor and one for a magnetized conductor. The latter scenario would require us to first remove the fixed internal magnetic field of the body and its interaction with surrounding plasma from the data, to identify the induced field. Modelling of the interaction between the solar wind and the body is an integral part of the magnetometer investigation and could be utilized in an electromagnetic sounding effort.

The uncertainties in Psyche's metallic content and porosity raise the possibility that Psyche would not be a good conductor, and its inductive response would be too weak for sounding. Even in this case, magnetometer data can be used to probe the internal structure. Bodies with conducting outer layers cause the magnetic field lines carried by the wind to pileup on their upwind side and drape behind them, as was observed around Venus (Kallio et al., 1998) and several comets, such as comet 1P/Haley (Israelevich & Ershkovich, 1994). On the other extreme are very good insulators, which allow the incoming magnetic field to diffuse through them and do not give rise to draping, as was observed around the Moon (Zhang et al., 2014). Asteroids may fall somewhere in between these two topologies. Simulations of chondritic asteroids in the ancient solar wind suggest they produce a pileup but, to a smaller degree, due to their higher resistivity (Oran et al., 2018). The magnetometer measurements would allow to infer whether the IMF drapes around Psyche. If there is no draping or pileup, this can place an upper limit on the conductivity. If some signature of draping is present, more detailed comparisons to simulations can be made to constrain the resistivity profile. We note that if draping is absent, it can only be inferred there is a thick and resistive outer layer (the Moon, e.g., has a conducting core but creates no draping or pileup). A conducting interior could only be revealed by sounding in this case.

Finally, there are limitations of applying electromagnetic sounding to Psyche. To minimize the number of a priori assumptions in inverting the magnetic field data to retrieve the conductivity, planetary bodies are usually treated as having a one-dimensional (radial) profile of density, porosity, iron fraction, and temperature (Verhoeven et al., 2005). This assumption may be less appropriate for Psyche, which has a triaxial shape. In addition, highly conducting minerals such as magnetite and pure metals such as iron have a strong inductive response, leading to higher secondary fields but, on the other hand, have small skin depths (Khurana et al., 2009). This limits the depth of penetration of external magnetic field variations, depending on their frequencies. Only slow-changing fields would penetrate deep into the body and can be used to probe deeper layers.

### 5.3. Crater Morphology

Crater morphology can further provide constraints on Psyche's bulk properties. Laboratory-scale impact experiments show that craters in manufactured iron-nickel ingots and iron meteorites exhibit a different morphology compared to craters in rocky targets. Notably, craters in metal have higher depth-to-diameter ratios and retain sharper rims than in rock, and their floors have characteristic "petal-like" morphologies (e.g., Libourel et al., 2019; Marchi et al., 2019). These structures may or may not be present at much larger scales, such as those relevant to Psyche's observations.

To first order, the morphology observed in lab impact experiments is primarily controlled by the high strength of metal (~500 MPa). This strength is typical for solid centimeter-scale metallic objects, such as Fe-Ni man-made alloys or iron meteorites (Marchi et al., 2019). At larger scale, however, strength could be significantly reduced by the presence of porosity and fractures. Nevertheless, some of the characteristic crater morphologies observed in lab experiments may be present on large craters, provided metal retains a high strength over distances comparable to the observed crater sizes. In addition, large craters are expected to undergo gravity-driven collapse at the end of the excavation phase. On high strength metallic bodies, collapse could be suppressed. If this is the case, then the morphology of craters in metal on Psyche could be very different than those on rocky targets, and will help the team discriminate metal from silicate-dominated regions.

Silicates could be endogenous to Psyche or due to deposition via rocky impactors. These two scenarios should result in different surface distributions of silicates. For instance, deposition via impacts tend to leave silicates within the crater floors (an outcome also seen in impact experiments; Daly & Schultz, 2018; Libourel et al., 2019; Marchi et al., 2019), while endogenous silicates are expected to be more broadly distributed at the surface. As a result, the two scenarios could also lead to different stratifications of the silicates in the near-

surface, which can be exposed and probed via cratering. Further, optical remote sensing provides compositional information about the upper microns of the body, whereas the gamma-ray and neutron spectrometer samples the composition to depths of decimeters (gamma rays) to meters (neutrons). Thus, surface contamination by later impacts might not be seen in the gamma-ray spectrometer but might be dominated in the optical data.

Crater morphology can also provide constraints to discriminate between craters produced by high velocity asteroids or low velocity reaccreted fragments. The latter, low relative velocity impacts, would be expected during reaccretion from a silicate-stripping event. Reaccretion is expected at a few  $100 \text{ m s}^{-1}$ , well below the average  $5 \text{ km s}^{-1}$  for asteroidal impactors. Also, reaccretion will take place shortly after the massive collision, when Psyche is expected to be strongly heated or molten. These impacts could lead to a very different crater morphology than typically observed on hypervelocity impacts on solid surfaces. In addition, images will be used to create a global geologic map of the surface, which will not only identify the geologic processes that produced surface materials but also the stratigraphic order in which they were emplaced, enabling recognition of the geologic history of Psyche.

The number and size distribution of large craters ( $>50 \text{ km}$ ) is expected to be particularly diagnostic for assessing Psyche's silicate versus metallic nature. For instance, a significant number of large craters on Psyche would suggest it has a low bulk strength (through consisting of silicate or highly fractured metal). On the other hand, a small number or lack of large craters would imply a high bulk strength (likely metal).

Available data of Psyche's shape indicate the presence of up to four cavities  $>50 \text{ km}$  on its surface (Shepard et al., 2017; Viikinkoski et al., 2018). This is compatible with the number of such craters predicted by current collision models for a time span of 4.5 Ga and for a bulk strength of  $\sim 50 \text{ MPa}$  (Marchi et al., 2019). This strength exceeds that of common hard rocks, such as basalts. Cratering studies alone cannot derive the whole-body bulk strength of Psyche, but it could be bound thanks to a synergistic approach with other remote observations, such as compositional information from gamma-ray spectrometer.

#### 5.4. Interior Structure Via Gravity Science

The Psyche mission will use a two-way X-band radio system (7.2 GHz uplink and 8.4 GHz downlink) to determine the gravity field of Psyche. If Psyche's structure predominantly reflects solidification from a liquid it may have a radially varying density structure. In contrast, if it was significantly disrupted and/or was never molten, it would be more dominated by a spatially varying density structure as well as random radial density variations.

Comparing the observed gravity and topography with models of assumed interior structures would indicate the degree of spherical symmetry or extent of breakage into rubble (R. S. Park et al., 2016). Both radial and azimuthal density variations within Psyche can be analyzed by computing the gravity-topography correlation (coherence), the response function between gravity and topography (admittance), and gravity anomaly maps (Ermakov et al., 2017; Konopliv et al., 2018; R. S. Park et al., 2014; Wieczorek et al., 2013). In addition, if there exist masses of reaccreted silicate provinces on top of a core, a degree 10 gravity field (i.e., half wavelength of  $\sim 35 \text{ km}$ ) might detect lower/higher gravity regions, indicative of structure and degree of spherical symmetry or breakage into rubble.

To demonstrate the expected recovery of Psyche's gravity field, we have performed a detailed simulation including the effects of realistic error sources, such as media calibration and nongravitational perturbations (R. Park et al., 2013). For the Doppler data accuracy, data with  $0.1 \text{ mm/s}$  at 60-s count time was considered, which is typical for deep-space missions (Konopliv et al., 2018; R. S. Park et al., 2016). All terrestrial bodies with a sufficiently known gravity field follow a power law relation, called the Kaula Rule (Kaula, 1966; Konopliv et al., 2011a; Zuber et al., 2012), which is a function of spherical harmonic degree (wavelength is proportional to  $1/n$ , where  $n$  is the spherical harmonic degree). For Psyche, the expected Kaula rule is  $0.05 \text{ n}^{-2}$  (Konopliv, Asmar, Bills, et al., 2011a). Based on this assumption, a simulation result shows that a degree and order 18 gravity field (i.e., half wavelength of  $\sim 20 \text{ km}$ ) for Psyche can be recovered with observations at the planned science orbits.

Psyche's topography will be determined by processing onboard imagery via a stereo reconstruction technique, such as stereo-photogrammetry or stereo-photoclinometry (R. S. Park et al., 2019). The resolution of

the recovered topography will be between 2 and 3 orders of magnitude better than the resolution of the recovered gravity field. Therefore, the accuracy of the gravity data (~20 km) will be the limiting factor for the interior modeling of Psyche. Knowledge of the shape and total mass of Psyche will improve the uncertainty of bulk density to better than 1%.

## 6. Conclusions

While some years ago the consensus was on Psyche being almost entirely metal, new data on density, radar properties, and spectral signatures indicate that the asteroid is something perhaps even more enigmatic: a mixed metal and silicate world. Based on existing data, we conclude that

- Psyche's bulk density appears to be between 3,400 and 4,100 kg m<sup>-3</sup> (see Table 2).
- Psyche is predicted to have between ~30 vol% metal (point D in Figure 3) and ~60 vol% metal (the high-metal end of the yellow oval in Figure 3).
- The reflectance and optical properties of Psyche indicate nonuniquely that the body may be largely metallic.
- The interpretation of a partial metal surface is supported by measurements of the body's density and radar albedo.
- Another major component is likely a low-Fe, low-Ca pyroxene indicated by a shallow (~0%–3%) absorption feature centered at ~0.919–0.950 μm.
- Impacts probably have left large concentrations of exogenous, perhaps hydrated chondritic, material randomly distributed on the surface, but likely correlated with impact craters.
- Pallasites and CB chondrites can match both Psyche's density, although typical pallasitic olivine contains too much iron to be consistent with the reflectance spectra of Psyche. Pyroxene pallasite remains an enticing possibility.
- Using density as a determiner, Psyche could consist of pallasitic material throughout. This case requires that pallasites formed as a relatively homogeneous mixture of silicate and metal via a hit-and-run collision between far larger bodies that simply spalls off a secondary body (Psyche) that is a mantle-core mixture.
- If, alternatively, pallasites are a veneer over a relatively intact iron-nickel metal core, such a body would require high porosity to match Psyche's density.
- Though their density is equivalent, mesosiderites are an unlikely analog to bulk Psyche, both because the parent body of the mesosiderites is not expected to be pure mesosiderite, and because mesosiderites have far more iron-rich silicates than Psyche appears to have.
- CB chondrites have appropriate density and magnesian silicates. If Psyche has remanent magnetization and matches the CB chondrites compositionally, then its parent body must have been either a mixture of a differentiated and a chondritic body, or a partially differentiated body with a chondritic crust.
- The science payload of the Psyche mission, which includes magnetometers, multispectral imagers, neutron spectrometer, and a gamma-ray spectrometer, will be able to distinguish among the possible Psyches outlined here.

## Acknowledgments

This work is supported by NASA contract NNM16AA09, "Psyche: Journey to a Metal World." The contribution of MAW was supported by the French Space Agency (CNES). The code and data used to generate Figure 3 are available in Wiczorek (2020), January 8). Elkins-Tanton conceptualized, supervised and then wrote portions of this paper. All other authors wrote portions of the original draft or reviewed and edited. Wiczorek, Polansky, and Park validated calculations.

## References

- Abe, S., Mukai, T., Hirata, N., Barnouin-Jha, O. S., Cheng, A. F., Demura, H., et al. (2006). Mass and local topography measurements of Itokawa by Hayabusa. *Science*, *312*(5778), 1344–1347. <https://doi.org/10.1126/science.1126272>
- Adams, J. B. (1975). Interpretation of visible and near-infrared diffuse reflectance spectra of pyroxenes and other rock-forming minerals. *Journal of Geophysical Research*, *79*, 4829–4836.
- Asphaug, E., Agnor, C. B., & Williams, Q. (2006). Hit-and-run planetary collisions. *Nature*, *439*(7073), 155–160. <https://doi.org/10.1038/nature04311>
- Baer, J., & Chesley, S. R. (2008). Astrometric masses of 21 asteroids, and an integrated asteroid ephemeris. *Celestial Mechanics and Dynamical Astronomy*, *100*, 27–42.
- Baer, J., & Chesley, S. R. (2017). Simultaneous mass determination for gravitationally coupled asteroids. *Astronomical Journal*, *154*(2).
- Baer, J., Chesley, S. R., & Matson, R. D. (2011). Astrometric masses of 26 asteroids and observations on asteroid porosity. *The Astronomical Journal*, *141*, 1–12.
- Bass, J. D. (1995). *Elasticity of minerals, glasses, and melts. In Mineral Physics and Crystallography: A Handbook of Physical Constants* (Vol. 2, pp. 45–63). Washington, D.C.: AGU Reference Shelf.
- Beck, A. W., Lawrence, D. J., Peplowski, P. N., Prettyman, T. H., McCoy, T. J., McSween, H. Y. Jr., et al. (2015). Using HED meteorites to interpret neutron and gamma-ray data from asteroid 4 Vesta. *Meteoritics and Planetary Science*, *50*(8), 1311–1337. <https://doi.org/10.1111/maps.12467>
- Beck, A. W., Lawrence, D. J., Peplowski, P. N., Viviano-Beck, C. E., Prettyman, T. H., McCoy, T. J., et al. (2017). Igneous lithologies on asteroid (4) Vesta mapped using gamma-ray and neutron data. *Icarus*, *286*, 35–45. <https://doi.org/10.1016/j.icarus.2017.01.008>

- Becker, T. M., Retherford, K. D., Roth, L., Hendrix, A. R., McGrath, M. A., Cunningham, N. J., et al. (2017). UV Observations and theory of the moon Europa and asteroid (16) Psyche. Paper presented at the American Geophysical Union, New Orleans.
- Bercovici, H. L., Elkins-Tanton, L. T., Schaefer, L., & O'Rourke, J. G. (2019). Planetesimal cores may come in many flavors; how oxidation state affects core sulfur content. Paper presented at the American Geophysical Union Fall Meeting, San Francisco, CA.
- Binzel, R. P., Bus, R., Schelte, J., Xu, S., Sunshine, J. M., & Burbine, T. H. (1995). Rotationally resolved spectra of asteroid 16 Psyche. *Icarus*, *117*, 443–445.
- Brearely, A. J., & Jones, R. H. (1998). Chondritic meteorites. In J. J. Papike (Ed.), *Planetary Materials, Mineralogical Association of American, Chantilly, Virginia*, (Vol. 36, pp. 31–398).
- Britt, D. T., & Consolmagno, S. J. (2003). Stony meteorite porosities and densities: A review of the data through 2001. *Meteoritics and Planetary Science*, *38*(8), 1161–1180.
- Britt, D. T., & Pieters, C. M. (1988). Bidirectional reflectance properties of iron-nickel meteorites. *Lunar and Planetary Science Conference*, *18*.
- Bryson, J. F. J., Harrison, J., Neufeld, A., Nimmo, F., Herrero-Albillos, J., Kronast, F., & Weiss, B. P. (2017). Paleomagnetic evidence for dynamo activity driven by inward crystallisation of a metallic core. *Earth and Planetary Science Letters*, *472*, 152–163.
- Bunch, T. E., Keil, K., & Olsen, E. (1970). Mineralogy and petrology of silicate inclusions in iron meteorites. *Contributions to Mineralogy and Petrology*, *25*, 297–340.
- Burbine, T. H., & Binzel, R. P. (2002). Small main-belt asteroid spectroscopic survey in the near-infrared. *Icarus*, *159*, 468–499.
- Bus, S. J., & Binzel, R. P. (2002). Phase II of the small main-belt asteroid spectroscopic survey: A feature-based taxonomy. *Icarus*, *158*, 146–177.
- Buseck, P. R. (1977). Pallasite meteorites—Mineralogy, petrology and geochemistry. *Geochemica et Cosmochimica Acta*, *41*, 711–721.
- Carry, B. (2012). Density of asteroids. *Planetary and Space Science*, *73*, 98–118.
- Chabot, N. L. (2004). Sulfur contents of the parental metallic cores of magmatic iron meteorites. *Geochimica Et Cosmochimica Acta*, *68*, 3607–3618.
- Clark, B. E., Bus, S. J., Rivkin, A. S., Shepard, M. K., & Shah, S. (2004). Spectroscopy of X-type asteroids. *The Astronomical Journal*, *128*, 3070–3081.
- Cloutis, E. A., Gaffey, M. J., Smith, D. G., & Lambert, R. S. J. (1990a). Metal silicate mixtures: Spectral properties and applications to asteroid taxonomy. *Journal of Geophysical Research*, *95*, 8323–8338.
- Cloutis, E. A., Gaffey, M. J., Smith, D. G., & Lambert, R. S. J. (1990b). Reflectance spectra of “featureless” materials and the surface mineralogies of M-and E-class asteroids. *Journal of Geophysical Research*, *95*(B1), 281–293.
- Cloutis, E. A., Hardersen, P. S., Reddy, V., Gaffey, M. J., Bailey, D., & Craig, M. A. (2009). Metal-orthopyroxene and metal-olivine mixtures: Spectral reflectance properties and implications for Asteroid Spectroscopy. *Lunar and Planetary Science Conference*, *40*.
- Cloutis, E. A., Izawa, M. R., & Beck, P. (2018). Reflectance spectroscopy of chondrites. In N. Abreu (Ed.), *Primitive Meteorites and Asteroids*, (pp. 73–343). Amsterdam:Elsevier.
- Connelly, J., Amelin, Y., Krot, A., & Bizzarro, M. (2008). Chronology of the Solar System's oldest solids. *The Astrophysical Journal Letters*, *675*(2), 121–124.
- Coradini, A., Capaccioni, F., Erard, S., Arnold, G., de Sanctis, M. C., Filacchione, G., et al. (2011). The surface composition and temperature of asteroid 21 Lutetia as observed by Rosetta/VIRTIS. *Science*, *334*(6055), 492–494. <https://doi.org/10.1126/science.1204062>
- Daly, R. T., & Schultz, P. H. (2018). Projectile preservation during oblique hypervelocity impacts. *Meteoritics and Planetary Science*, *53*, 1364–1390.
- Delbo, M., Libourel, G., Wilkerson, J., Murdoch, N., Michel, P., Ramesh, K. T., et al. (2014). Thermal fatigue as the origin of regolith on small asteroids. *Nature*, *508*, 233–236.
- Delbo, M., Mueller, M., Emery, J., Rozitis, B., & Capria, M. T. (2015). Asteroid thermo-physical modeling. In P. Michel, F. E. DeMeo, & W. F. Bottke (Eds.), *Asteroids IV*, (pp. 107–128). Tucson, AZ: The University of Arizona Press.
- DeMeo, F. E., Binzel, R. P., Slivan, S. M., & Bus, S. J. (2009). An extension of the Bus asteroid taxonomy into the near-infrared. *Icarus*, *202*, 160–180.
- Descamps, P., Marchis, F., Berthier, J., Emery, J. P., Duchêne, G., de Pater, I., et al. (2011). Triplicity and physical characteristics of Asteroid (216) Kleopatra. *Icarus*, *211*(2), 1022–1033. <https://doi.org/10.1016/j.icarus.2010.11.016>
- Dollfus, A., Mandeville, J.-C., & Duseaux, M. (1979). The nature of the M-type asteroids from optical polarimetry. *Icarus*, *37*, 124–132.
- Domingue, D. L., Vilas, F., Holsclaw, G. M., Warell, J., Izenberg, N. R., Murchie, S. L., et al. (2010). Whole-disk spectrophotometric properties of Mercury: Synthesis of MESSENGER and ground-based observations. *Icarus*, *209*(1), 101–124. <https://doi.org/10.1016/j.icarus.2010.02.022>
- Drummond, J. D., Merline, W. J., Carry, B., Conrad, A., Reddy, V., Tamblyn, P., et al. (2018). The triaxial ellipsoid size, density, and rotational pole of asteroid (16) Psyche from Keck and Gemini AO observations 2004–2015. *Icarus*, *305*, 174–185. <https://doi.org/10.1016/j.icarus.2018.01.010>
- Dyal, P., & Parkin, C. W. (1973). Global electromagnetic induction in the moon and planets. *Physics of the Earth and Planetary Interiors*, *7*, 251–265.
- Elkins Tanton, L. T., Weiss, B. P., & Zuber, M. T. (2011). Chondrites as samples of differentiated planetesimals. *Earth and Planetary Science Letters*, *305*, 1–10.
- Elkins-Tanton, L. T. (2016). The taxonomy of planetesimals: Consequences for planets. In L. T. Elkins-Tanton, & B. P. Weiss (Eds.), *Planetesimals: Early Differentiation and Consequences for Planets*, (pp. 365–375). Cambridge, UK: Cambridge University Press.
- Ermakov, A. I., Fu, R. R., Castillo-Rogez, J. C., Raymond, C. A., Park, R. S., Preusker, F., et al. (2017). Constraints on Ceres internal structure and evolution from its shape and gravity measured by the Dawn spacecraft. *Journal of Geophysical Research: Planets*, *122*, 2267–2293. <https://doi.org/10.1002/2017JE005302>
- Ermakov, A. I., Zuber, M. T., Smith, D. E., Raymond, C. A., Balmino, G., Fu, R. R., & Ivanov, B. A. (2014). Constraints on Vesta's interior structure using gravity and shape models from the Dawn mission. *Icarus*, *240*, 146–160.
- Fienga, A., Laskar, J., Morley, T., Manche, H., Kuchynka, P., le Poncin-Lafitte, C., et al. (2009). INPOP08, a 4-D planetary ephemeris: From asteroid and time-scale computations to ESA Mars Express and Venus Express contributions. *Astronomy and Astrophysics*, *507*(3), 1675–1686. <https://doi.org/10.1051/0004-6361/200911755>
- Fienga, A., Manche, H., Laskar, J., Gastineau, M., & Verma, A. (2014). INPOP new release: INPOP13c. Arxiv ID: 1301.1510.
- Fish, R. A., Goles, G. G., & E., A. (1960). The record in meteorites III. On the development of meteorites in asteroidal bodies. *The Astrophysical Journal*, *132*, 243–258.
- Flynn, G. J., Consolmagno, G. J., Brown, P., & Macke, R. J. (2018). Physical properties of the stone meteorites: Implications for the properties of their parent bodies. *Chemie der Erde*, *78*, 269–298.

- Fornasier, S., Clark, B. E., Dotto, E., Migliorini, A., Ockert-Bell, M., & Barucci, M. A. (2010). Spectroscopic survey of M-type asteroids. *Icarus*, *210*, 655–673.
- Gaffey, M. J. (1976). Spectral reflectance characteristics of the meteorite classes. *Journal of Geophysical Research*, *81*, 905–920.
- Goldstein, J. I., Scott, E. R. D., & Chabot, N. L. (2009). Iron meteorites: Crystallization, thermal history, parent bodies, and origin. *Chemie der Erde*, *69*, 293–325.
- Hanuš, J., Delbo, M., Ďurech, J., & Ali-Lagoa, V. (2018). Thermophysical modeling of main-belt asteroids from WISE thermal data. *Icarus*, *309*, 297–337.
- Hanuš, J., Viikinkoski, M., Marchis, F., Ďurech, J., Kaasalainen, M., Delbo, M., et al. (2017). Volumes and bulk densities of forty asteroids from ADAM shape modeling. *Astronomy and Astrophysics*, *601*, A114. <https://doi.org/10.1051/0004-6361/201629956>
- Hardersen, P. S., Cloutis, E. A., Reddy, V., Mothé-Diniz, T., & Emery, J. P. (2011). The M-/X-asteroid menagerie: Results of an NIR spectral survey of 45 main-belt asteroids. *Meteoritics and Planetary Science*, *46*, 1910–1938.
- Hardersen, P. S., Gaffey, M. J., & Abell, P. A. (2005). Near-IR spectral evidence for the presence of iron-poor orthopyroxenes on the surfaces of six M-type asteroids. *Icarus*, *175*, 141–158.
- Hart, W., Brown, G. M., Collins, S., de Soria, M., Fieseler, P., Goebel, D., et al. (2018). Overview of the spacecraft design for the Psyche mission concept. Paper presented at the 39th IEEE Aerospace Conference, Big Sky, MT.
- Hartzell, C. M., & Scheeres, D. J. (2013). Dynamics of levitating dust particles near asteroids and the Moon. *Journal of Geophysical Research: Planets*, *118*, 116–125. <https://doi.org/10.1029/2012JE004162>
- Herique, A., Agnus, B., Asphaug, E., Barucci, A., Beck, P., Bellrose, J., et al. (2018). Direct observations of asteroid interior and regolith structure: Science measurement requirements. *Advances in Space Research*, *62*(8), 2141–2162. <https://doi.org/10.1016/j.asr.2017.10.020>
- Hood, L. L., Mitchell, D. L., Lin, R. P., Acuna, M. H., & Binder, A. B. (1999). Initial measurements of the lunar induced dipole moment using Lunar Prospector magnetometer data. *Geophysical Research Letters*, *26*, 2327–2330.
- Hunt, G. R., & Salisbury, J. W. (1970). Visible and near-infrared spectra of minerals and rocks: I Silicate minerals. *Modern Geology*, *1*, 283–300.
- Israelevich, P. L., & Ershkovich, A. I. (1994). Induced magnetosphere of comet Halley. 2: Magnetic field and electric currents. *Journal of Geophysical Research*, *99*, 21.
- Jarosewich, E. (1990). Chemical analyses of meteorites: A compilation of stony and iron meteorite analyses. *Meteoritics*, *25*, 323–337.
- Johnson, B. C., Sori, M. M., & Evans, A. J. (2019). Ferrovolcanism on metal worlds and the origin of pallasites. *Nature Astronomy*.
- Jones, J. H., & Drake, M. J. (1983). Experimental investigations of trace element fractionation in iron meteorites, II: The influence of sulfur. *Geochimica et Cosmochimica Acta*, *47*, 1199–1209.
- Kallio, E., Luhmann, J. G., & Lyon, J. G. (1998). Magnetic field near Venus—A comparison between Pioneer Venus Orbiter magnetic field observations and an MHD simulation. *Journal of Geophysical Research*, *103*, 4723.
- Kaula, W. M. (1966). *Theory of satellite Geodesy*. Waltham, MA: Blaisdell.
- Khurana, K. K., Kivelson, M. G., Hand, K. P., & Russell, C. T. (2009). Electromagnetic induction from Europa's ocean and the deep interior. In R. T. Pappalardo, W. B. McKinnon, & K. K. Khurana (Eds.), *Europa*, (pp. 572–586). Tucson, AZ: University of Arizona Press.
- Kochetova, O. M. (2004). Determination of large asteroid masses by the dynamical method. *Solar System Research*, *38*(1), 66–75.
- Konopliv, A. S., Asmar, S. W., Bills, B. G., Mastrodemos, N., Park, R. S., Raymond, C. A., et al. (2011a). The Dawn gravity investigation at Vesta and Ceres. In C. Russell, & C. Raymond (Eds.), *The Dawn Mission to Minor Planets 4 Vesta and 1 Ceres*, (pp. 461–486). New York, NY: Springer. [https://doi.org/10.1007/978-1-4614-4903-4\\_15](https://doi.org/10.1007/978-1-4614-4903-4_15)
- Konopliv, A. S., Asmar, S. W., Bills, B. G., Mastrodemos, N., Park, R. S., Raymond, C. A., et al. (2011b). The Dawn mission to minor planets 4 Vesta and 1 Ceres. In C. Russell, & C. Raymond (Eds.), *The Dawn Mission to Minor Planets 4 Vesta and 1 Ceres*, (pp. 461–486). New York, N.Y.: Springer. [https://doi.org/10.1007/978-1-4614-4903-4\\_15](https://doi.org/10.1007/978-1-4614-4903-4_15)
- Konopliv, A. S., Asmar, S. W., Folkner, W. M., Karatekin, O., Nunes, D. C., Smrekar, S. E., et al. (2011). Mars high resolution gravity fields from MRO, Mars seasonal gravity, and other dynamical parameters. *Icarus*, *211*(1), 401–428. <https://doi.org/10.1016/j.icarus.2010.10.004>
- Konopliv, A. S., Park, R. S., Vaughan, A. T., Bills, B. G., Asmar, S. W., Ermakov, A. I., et al. (2018). The Ceres gravity field, spin pole, rotation period and orbit from the Dawn radiometric tracking and optical data. *Icarus*, *299*, 411–429. <https://doi.org/10.1016/j.icarus.2017.08.005>
- Kring, D. A., Hill, D. H., Gleason, J. D., Britt, D. T., Consolmagno, G. J., Farmer, M., et al. (1999). Portales Valley: A meteoritic sample of the brecciated and metal-veined floor of an impact crater on an H-chondrite asteroid. *Meteoritics and Planetary Science*, *34*(4), 663–669. <https://doi.org/10.1111/j.1945-5100.1999.tb01372.x>
- Krot, A., Amelin, Y., Cassen, P., & Meibom, A. (2005). Young chondrules in CB chondrites from a giant impact in the early Solar System. *Nature*, *436*(7053), 989–992. <https://doi.org/10.1038/nature03830>
- Kuchynka, P., & Folkner, W. M. (2013). A new approach to determining asteroid masses from planetary range measurements. *Icarus*, *222*, 243–253.
- Kuzmanoski, M., & Koračević, A. (2002). Motion of the asteroid (13206) 1997GC22 and the mass of (16) Psyche. *Astronomy and Astrophysics*, *395*, L17–L19.
- Landsman, Z. A., Emery, J. P., Campins, H., Hanuš, J., Lim, L. F., & Cruikshank, D. P. (2018). Asteroid (16) Psyche: Evidence for a silicate regolith from spitzer space telescope spectroscopy. *Icarus*, *304*, 58–73.
- Langseth, M. G., Keihm, S. J., & Peteres, K. (1976). Revised lunar heat-flow values. *Proceeding of the Lunar Science Conference*, *7*, 3143–3171.
- Libourel, G., Nakamura, A. M., Beck, P., Potin, S., Ganino, C., Jacomet, S., et al. (2019). Hypervelocity impacts as a source of deceiving surface signatures on iron-rich asteroids. *Science Advances*, *5*(8), eaav3971. <https://doi.org/10.1126/sciadv.aav3971>
- Lupishko, D. F., & Belskaya, I. N. (1989). Om the surface composition of the M-type asteroids. *Icarus*, *78*, 395–401.
- Macke, R. J. (2010). Survey of meteorite physical properties: Density, porosity and magnetic susceptibility. (Ph.D.), University of Central Florida.
- Magri, C., Nolan, M. C., Ostro, S. J., & Giorgini, J. D. (2007). A radar survey of main-belt asteroids: Arecibo observations of 55 objects during 1999-2003. *Icarus*, *186*, 126–151.
- Marchi, S., Durda, D. D., Polanskey, C. A., Asphaug, E., Bottke, W. F., Elkins-Tanton, L. T., et al. (2019). Hypervelocity impact experiments in iron-nickel ingots and meteorites: Implications for the NASA Psyche mission. *Journal of Geophysical Research: Planets*.
- Matter, A., Delbo, M., Carry, B., & Ligori, S. (2013). Evidence of a metal-rich surface for the Asteroid (16) Psyche from interferometric observations in the thermal infrared. *Icarus*, *226*, 419–427.
- Maurel, C., Bryson, J. F. J., Weiss, B. P., Lyons, R. J., Ball, M. R., Chopdekar, R. V., & Scholl, A. (2019). Partial differentiation and magnetic history of the IIE iron meteorite parent body, Paper presented at the Lunar and Planetary Science Conference, The Woodlands, TX.

- McClintock, W. E., Izenberg, N. R., Holsclaw, G. M., Blewett, D. T., Domingue, D. L., Head, J. W., et al. (2008). Spectroscopic observations of Mercury's surface reflectance during MESSENGER's first Mercury flyby. *Science*, *321*(5885), 62–65. <https://doi.org/10.1126/science.1159933>
- Mittlefehldt, D. W., McCord, T. J., Goodrich, C. A., & Kracher, A. (1998). Non-chondritic meteorites from asteroidal bodies. In J. J. Papike (Ed.), *Planetary Materials*, (Vol. 36, pp. 195–233). Washington DC: Mineralogical Society of America.
- Nittler, L. R., McCoy, T. J., Clark, P. E., Murphy, M. E., Trombka, J. I., & Jarosewich, E. (2004). Bulk element compositions of meteorites: A guide for interpreting remote-sensing geochemical measurements of planets and asteroids. *Antarctic Meteorite Research*, *17*, 233–253.
- Ockert-Bell, M. E., Clark, B. E., Shepard, M. K., Isaacs, R. A., Cloutis, E. A., Fornasier, S., & Bus, S. J. (2010). The composition of M-type asteroids: Synthesis of spectroscopic and radar observations. *Icarus*, *210*, 674–692.
- Olsen, N. (1999). Induction studies with satellite data. *Surveys in Geophysics*, *20*, 309–340.
- Opeil, C. P., Consolmagno, G. J., Safarik, D. J., & Britt, D. T. (2012). Stony meteorite thermal properties and their relationship with meteorite chemical and physical state. *Meteoritics and Planetary Science*, *47*, 319–329.
- Oran, R., Weiss, B. P., & Cohen, O. (2018). Were chondrites magnetized by the early solar wind? *Earth and Planetary Science Letters*, *492*, 222.
- Oran, R., Weiss, B. P., & de Soria-Santacruz Pic, M. (2018). *On the possibility of asteroid magnetospheres*. Washington, DC: Paper presented at the American Geophysical Union Fall Meeting.
- Ormel, C. W., & Klahr, H. H. (2010). The effect of gas drag on the growth of protoplanets: Analytical expressions of the accretion of small bodies in laminar disks. *Astronomy & Astrophysics*, *520*, A43.
- Ostro, S. J. (1993). Planetary radar astronomy. *Reviews in Modern Physics*, *65*, 1235–1279.
- Ostro, S. J., Campbell, D. B., Chandler, J. F., Hine, A. A., Hudson, R. S., Rosema, K. D., & Shapiro, I. I. (1991). Asteroid 1986 DA: Radar evidence for a metallic composition. *Science*, *252*, 1399–1404.
- Park, R., Asmar, S. W., Fahnestock, E. G., Konopliv, A. S., Lu, W., & Watkins, M. M. (2013). Gravity recovery and interior laboratory simulations of static and temporal gravity field. *Journal of Spacecraft and Rockets*, *49*, 390–400.
- Park, R. S., Konopliv, A. S., Asmar, S. W., Bills, B. G., Gaskell, R. W., Raymond, C. A., et al. (2014). Gravity field expansion in ellipsoidal harmonic and polyhedral internal representations applied to Vesta. *Icarus*, *240*, 118–132. <https://doi.org/10.1016/j.icarus.2013.12.005>
- Park, R. S., Konopliv, A. S., Bills, B. G., Rambaux, N., Castillo-Rogez, J. C., Raymond, C. A., et al. (2016). A partially differentiated interior for Ceres deduced from its gravity field and shape. *Nature*, *537*(7621), 515–517. <https://doi.org/10.1038/nature18955>
- Park, R. S., Vaughan, A. T., Konopliv, A. S., Ermakov, A. I., Mastrodomos, N., Castillo-Rogez, J. C., et al. (2019). High-resolution shape model of Ceres from stereophotoclinometry using Dawn Imaging Data. *Icarus*, *319*, 812–827. <https://doi.org/10.1016/j.icarus.2018.10.024>
- Peplowski, P. N., Bazell, D., Evans, L. G., Goldsten, J. O., Lawrence, D. J., & Nittler, L. R. (2015). Hydrogen and major element concentrations on 433 Eros: Evidence for an L- or LL-chondrite-like surface composition. *Meteoritics and Planetary Science*, *50*, 353–367.
- Peplowski, P. N., Beck, A. W., & Lawrence, D. J. (2016). Geochemistry of the lunar highlands as revealed by measurements of thermal neutrons. *Journal of Geophysical Research: Planets*, *121*, 388–401. <https://doi.org/10.1002/2015JE004950>
- Polanskey, C. A., Elkins-Tanton, L., Jaumann, R., Lawrence, D. J., Marsh, D. M., Moore, R. R., (2018a). Psyche science operations concept: Maximize reuse to minimize risk. Paper presented at the 2018 SpaceOps Conference.
- Polanskey, C. A., Elkins-Tanton, L., Jaumann, R., Lawrence, D. J., Marsh, D. M., Moore, R. R., et al. (2018b). Psyche science operations: Maximize reuse to minimize risk. Paper presented at the American Institute of Aeronautics and Astronautics.
- Prettyman, T. H., Hagerty, J. J., Elphic, R. C., Feldman, W. C., Lawrence, D. J., McKinney, G. W., & Vaniman, D. T. (2006). Elemental composition of the lunar surface: Analysis of gamma ray spectroscopy data from Lunar Prospector. *Journal of Geophysical Research*, *111*, E12007. <https://doi.org/10.1029/2005JE002656>
- Prettyman, T. H., Mittlefehldt, D. W., Yamashita, N., Lawrence, D. J., Beck, A. W., Feldman, W. C., et al. (2012). Elemental mapping by Dawn reveals exogenic H in Vesta's regolith. *Science*, *338*(6104), 242–246. <https://doi.org/10.1126/science.1225354>
- Rivkin, A. S., Howell, E. S., Britt, D. T., Lebofsky, L. A., Nolan, M. C., & Branston, D. D. (1995). 3- $\mu$ m spectrophotometric survey of M- and E-class asteroids. *Icarus*, *117*, 90–100.
- Rivkin, A. S., Howell, E. S., Lebofsky, L. A., Clark, B. E., & Britt, D. T. (2000). The nature of M-class asteroids from 3- $\mu$ m observations. *Icarus*, *145*, 351–368.
- Russell, C. T., Coleman, P. J., & Goldstein, B. E. (1981). Measurements of the lunar induced magnetic moment in the geomagnetic tail: Evidence for a lunar core. *Planetary Science Conference*, *12*, 831–836.
- Russell, C. T., Raymond, C. A., Coradini, A., McSween, H. Y., Zuber, M. T., Nathues, A., et al. (2012). Dawn at Vesta: Testing the protoplanetary paradigm. *Science*, *336*(6082), 684–686. <https://doi.org/10.1126/science.1219381>
- Sanchez, J. A., Reddy, V., Shepard, M. K., Thomas, C., Cloutis, E. A., Takir, D., et al. (2017). Detection of rotational spectral variation on the M-type asteroid (16) Psyche. *The Astronomical Journal*, *153*(29).
- Scheeres, D. J., Britt, D., Carry, B., & Holsapple, K. A. (2015). Asteroid interiors and morphology. In P. Michel, F. DeMeo, & W. F. Bottke (Eds.), *Asteroids IV*, (pp. 745–766). Tucson, AZ: University of Arizona.
- Scheinberg, A., Fu, R. R., Elkins-Tanton, L. T., Weiss, B. P., & Stanley, S. (2017). Magnetic fields on asteroids and planetesimals. In L. T. Elkins-Tanton, & B. P. Weiss (Eds.), *Planetesimals: Early Differentiation and Consequences for Planets*, (pp. 180–203). Cambridge, UK: Cambridge University Press.
- Scherstén, A., Elliott, T., Hawkesworth, C., Russell, S., & Masarik, J. (2006). Hf–W evidence for rapid differentiation of iron meteorite parent bodies. *Earth and Planetary Science Letters*, *241*(3–4), 530–542.
- Scott, E. R. D., Haack, H., & McCoy, T. J. (1996). Core crystallization and silicate-metal mixing in the parent body of the IVA iron and stony-iron meteorites. *Geochimica et Cosmochimica Acta*, *60*, 1615–1631.
- Shepard, M. K., Richardson, J., Taylor, P. A., Rodriguez-Ford, L. A., Conrad, A., de Pater, I., et al. (2017). Radar observations and shape model of asteroid 16 Psyche. *Icarus*, *281*, 388–403. <https://doi.org/10.1016/j.icarus.2016.08.011>
- Shepard, M. K., Taylor, P. A., Nolan, M. C., Howell, E. S., Springmann, A., Giorgini, J. D., et al. (2015). A radar survey of M- and X-class asteroids. III. Insights into their composition, hydration state, & structure. *Icarus*, *245*, 38–55. <https://doi.org/10.1016/j.icarus.2014.09.016>
- Shepard, M. K., Timerson, B., Scheeres, D. J., Benner, L. A. M., Giorgini, J. D., Howell, E. S., et al. (2018). A revised shape model of asteroid (216) Kleopatra. *Icarus*, *311*, 197–209. <https://doi.org/10.1016/j.icarus.2018.04.002>
- Siltala, L., & Granvik, M. (2019). Asteroid mass estimation with the robust adaptive Metropolis algorithm. *Astronomy & Astrophysics*, *633*.

- Smyth, J. R., & McCormick, T. C. (1995). *Crystallographic data for minerals*. In *Mineral Physics & Crystallography: A Handbook of Physical Constants*, (Vol. 2, pp. 1–17). Washington, D.C: AGU Reference Shelf.
- Somenzi, L., Fienga, A., Laskar, J., & Kuchynka, P. (2010). Determination of asteroid masses from their close encounters with Mars. *Planetary and Space Science*, 58, 858–863.
- Spencer, J. R., Lebofsky, L. A., & Sykes, M. V. (1989). Systematic biases in radiometric diameter determinations. *Icarus*, 78, 337–354.
- Sunshine, J. M., & Pieters, C. M. (1998). Determining the composition of olivine from reflectance spectroscopy. *Journal of Geophysical Research*, 103, 13675–13688.
- Takir, D., Reddy, V., Sanchez, J., Shepard, M. K., & Emery, J. (2016). Detection of water and/or hydroxyl on asteroid (16) Psyche. *The Astronomical Journal*, 153, 31–37.
- Tholen, D. J. (1984). Asteroid taxonomy from cluster analysis of photometry. (Ph.D.), University of Arizona, Tucson, AZ.
- Trigo-Rodríguez, J. M., Moyano-Camero, C. E., Llorca, J., Fornasier, S., Barucci, M. A., Belskaya, I., et al. (2013). UV to far-IR reflectance spectra of carbonaceous chondrites—I. Implications for remote characterization of dark primitive asteroids targeted by sample-return missions. *Monthly Notices of the Royal Astronomical Society*, 437, 227–240.
- Urey, H. C. (1955). The cosmic abundances of potassium, uranium, and thorium and the heat balance of the Earth, the Moon, and Mars. *Proceedings of the National Academy of Sciences*, 41, 127–144.
- Usui, T., & McSween, H. Y. Jr. (2007). Geochemistry of 4 Vesta based on HED meteorites: Prospective study for interpretation of gamma ray and neutron spectra for the Dawn mission. *Meteoritics and Planetary Science*, 42, 255–269.
- Verhoeven, O., Rivoldini, A., Vacher, P., Mocquet, A., Choblet, G., Menvielle, M., & Lognonné, P. (2005). Interior structure of terrestrial planets: Modeling Mars' mantle and its electromagnetic, geodetic, and seismic properties. *Journal of Geophysical Research*, 110, E04009. <https://doi.org/10.1029/2004JE002271>
- Vernazza, P., Lamy, P., Groussin, O., Hiroi, T., Jorda, L., King, P. L., et al. (2011). Asteroid (21) Lutetia as a remnant of Earth's precursor planetesimals. *Icarus*, 216(2), 650–659. <https://doi.org/10.1016/j.icarus.2011.09.032>
- Viateau, B. (2000). Mass and density of asteroids (16) Psyche and (121) Hermione. *Astronomy and Astrophysics*, 354, 725–731.
- Viikinkoski, M., Vernazza, P., Hanuš, J., le Coroller, H., Tazhenova, K., Carry, B., et al. (2018). (16) Psyche: A mesosiderite-like asteroid? *Astronomy and Astrophysics*, 619, L3. <https://doi.org/10.1051/0004-6361/201834091>
- Walsh, K. J. (2018). Rubble pile asteroids. *Annual Review of Astronomy and Astrophysics*, 56, 593–624.
- Wasson, J. (1990). Ungrouped iron meteorites in Antarctica: Origin of anomalously high abundance. *Science*, 249, 900–902.
- Watanabe, S., Hirabayashi, M., Hirata, N., Hirata, N., Noguchi, R., Shimaki, Y., et al. (2019). Hayabusa2 arrives at the carbonaceous asteroid 162173 Ryugu—A spinning top-shaped rubble pile. *Science*, 339.
- Weidenschilling, S. J. (1978). Iron/silicate fractionation and the origin of Mercury. *Icarus*, 35, 99–111.
- Weisberg, M. K., McCoy, T. J., & Krot, A. N. (2006). Systematics and evaluation of meteorite classification. In D. S. Lauretta, & H. Y. McSween, Jr. (Eds.), *Meteorites and the Early Solar System*, (pp. 19–52). Tucson, AZ: University of Arizona Press.
- Weiss, B. P., & Elkins Tanton, L. T. (2013). Differentiated planetesimals and the parent bodies of chondrites. *Annual Review of Earth and Planetary Sciences*, 41, 529–560.
- Weiss, B. P., Gattacceca, J., Stanley, S., Rochette, P., & Christensen, U. R. (2010). Paleomagnetic records of meteorites and early planetesimal differentiation. *Space Science Reviews*, 152, 341–390.
- Wieczorek, M. A. (2020). Interpretation of the bulk density of (16) Psyche as a mixture of iron-nickel metal, a non-metal component, and porosity. *Zenodo*. <http://doi.org/10.5281/zenodo.3601007>
- Wieczorek, M. A., Neumann, G. A., Nimmo, F., Kiefer, W. S., Taylor, G. J., Melosh, H. J., et al. (2013). The crust of the Moon as seen by GRAIL. *Science*, 339(6120), 671–675. <https://doi.org/10.1126/science.1231530>
- Yang, J., Goldstein, J. I., & Scott, E. R. D. (2007). Iron meteorite evidence for early formation and catastrophic disruption of protoplanets. *Nature*, 446(7138), 888–891. <https://doi.org/10.1038/nature05735>
- Yang, J., Goldstein, J. I., & Scott, E. R. D. (2010). Main-group pallasites: Thermal history, relationship to IIIAB irons, and origin. *Geochimica et Cosmochimica Acta*, 74, 4471–4492.
- Zhang, H., Khurana, K. K., Kivelson, M. G., Angelopoulos, V., Wan, W. X., Liu, L. B., et al. (2014). Three-dimensional lunar wake reconstructed from ARTEMIS data. *Journal of Geophysical Research: Space Physics*, 119, 5220–5243. <https://doi.org/10.1002/2014JA020111>
- Zuber, M. T., Smith, D. E., Watkins, M. M., Asmar, S. W., Konopliv, A. S., Lemoine, F. G., et al. (2012). Gravity field of the Moon from the Gravity Recovery and Interior Laboratory (GRAIL) mission. *Science*, 339, 668–671.

## Erratum

In the originally published version of this article, there was a typographical error in Table 2. This error has since been corrected, and this version may be considered the authoritative version of record.